cmgh
CELLULAR AND MOLECULAR GASTROENTEROLOGY AND HEPATOLOGY

ORIGINAL RESEARCH

Disruption of FOXP3–EZH2 Interaction Represents a Pathobiological Mechanism in Intestinal Inflammation

Adebowale O. Bamidele,[1] Phyllis A. Svingen,[1] Mary R. Sagstetter,[1] Olga F. Sarmento,[1] Michelle Gonzalez,[1] Manuel B. Braga Neto,[1] Subra Kugathasan,[2] Gwen Lomberk,[3] Raul A. Urrutia,[3] and William A. Faubion Jr[1]

[1]*Epigenetics and Chromatin Dynamics Laboratory, Division of Gastroenterology and Hepatology and Translational Epigenomic Program, Center for Individualized Medicine, Mayo Clinic, Rochester, Minnesota;* [2]*Department of Pediatrics, Emory University, School of Medicine, Atlanta, Georgia;* [3]*Department of Surgery, Medical College of Wisconsin, Milwaukee, Wisconsin*

SUMMARY

We provide evidence that the physical and functional interaction between forkhead box protein 3 and enhancer of zeste homolog 2 necessary for regulatory T-cell–suppressive function can be impaired by inflammatory bowel disease–associated mutation or interleukin 6 signaling.

BACKGROUND & AIMS: Forkhead box protein 3 (FOXP3)$^+$ regulatory T cell (Treg) dysfunction is associated with autoimmune diseases; however, the mechanisms responsible for inflammatory bowel disease pathophysiology are poorly understood. Here, we tested the hypothesis that a physical interaction between transcription factor FOXP3 and the epigenetic enzyme enhancer of zeste homolog 2 (EZH2) is essential for gene co-repressive function.

METHODS: Human FOXP3 mutations clinically relevant to intestinal inflammation were generated by site-directed mutagenesis. T lymphocytes were isolated from mice, human blood, and lamina propria of Crohn's disease (CD) patients and non-CD controls. We performed proximity ligation or a co-immunoprecipitation assay in FOXP3-mutant$^+$, interleukin 6 (IL6)-treated or CD-CD4$^+$ T cells to assess FOXP3–EZH2 protein interaction. We studied *IL2* promoter activity and chromatin state of the interferon γ locus via luciferase reporter and chromatin-immunoprecipitation assays, respectively, in cells expressing FOXP3 mutants.

RESULTS: EZH2 binding was abrogated by inflammatory bowel disease–associated FOXP3 cysteine 232 (C232) mutation. The C232 mutant showed impaired repression of *IL2* and diminished EZH2-mediated trimethylation of histone 3 at lysine 27 on interferon γ, indicative of compromised Treg physiologic function. Generalizing this mechanism, IL6 impaired FOXP3–EZH2 interaction. IL6-induced effects were reversed by Janus kinase 1/2 inhibition. In lamina propria–derived CD4$^+$T cells from CD patients, we observed decreased FOXP3–EZH2 interaction.

CONCLUSIONS: FOXP3–C232 mutation disrupts EZH2 recruitment and gene co-repressive function. The proinflammatory cytokine IL6 abrogates FOXP3–EZH2 interaction. Studies in lesion-derived CD4$^+$ T cells have shown that reduced FOXP3–EZH2 interaction is a molecular feature of CD patients. Destabilized FOXP3–EZH2 protein interaction via diverse mechanisms and consequent Treg abnormality may drive gastrointestinal inflammation. *(Cell Mol Gastroenterol Hepatol 2019;7:55–71; https://doi.org/10.1016/j.jcmgh.2018.08.009)*

Keywords: Proinflammatory Cytokine; Epigenetics; Regulatory T Cells; Crohn's Disease.

Autoimmune diseases are known to share similar pathways and mechanisms of pathogenesis as shown through genomewide association studies.[1] Specifically, dysregulation of the host immunity, triggered by complex interactions between genetics, environmental factors, and the gut microbiota, is associated with inflammatory bowel disease (IBD) and extraintestinal manifestations.[2,3] As a result, in IBD patients, increased production of proinflammatory cytokines, including interleukin (IL)6, are known to contribute to disease pathogenesis.[4–9] Despite advances in mechanistic insight, a significant proportion of IBD patients remain refractory to our most effective biologic therapies, thus suggesting a role for other unknown pathophysiological mechanisms.[10,11]

X-chromosome–encoded forkhead domain-containing protein (FOXP3) is the lineage-defining oligomeric transcription factor required for the development of CD4$^+$CD25^{high} FOXP3$^+$ regulatory T cells (Tregs).[12] Tregs derived from the thymus during T-cell development (natural Tregs) or induced in the periphery are both necessary for maintaining immunologic self-tolerance and homeostasis

Abbreviations used in this paper: **CD, Crohn's disease; ChIP, chromatin-immunoprecipitation; co-IP, co-immunoprecipitation; C232, cysteine 232; EED, embryonic ectoderm development; EZH2, enhancer of zeste homolog 2; FCS, fetal calf serum; FOXP3, forkhead domain-containing X-chromosome–encoded protein; H3K27me3, trimethylated histone H3 at lysine 27; IBD, inflammatory bowel disease; IL, interleukin; IPEX, immune dysregulation, polyendocrinopathy, enteropathy, X-linked; JAK, Janus kinase; LZ, leucine zipper; PBMC, peripheral blood mononuclear cell; PBS, phosphate-buffered saline; PLA, proximity ligation assay; PMA, phorbol 12-myristate 13-acetate; PRC2, polycomb repressive complex 2; STAT, signal transducer and activator of transcription; SUZ12, suppressor of zeste; Th, T helper; Treg, regulatory T cell; WT, wild-type.**

Most current article

2352-345X
https://doi.org/10.1016/j.jcmgh.2018.08.009

by restraining pathologic immune responses including autoimmunity, inflammation, and allergy.[13] FOXP3 deletion or mutation can result in multi-organ autoimmunity in mice[14,15] and human immune dysregulation, polyendocrinopathy, enteropathy, X-linked (IPEX).[16,17] The immunosuppressive function of Tregs is maintained through a FOXP3-driven gene transcriptional program.[18] The functional capacity of FOXP3, such as gene repression, critically relies on its protein–protein interactions with a broad range of cofactors via its structural domains, as shown by mass spectrometric analysis.[19] These include sequence-specific transcription factors, chromatin modifiers, and FOXP3 itself.[20–25]

Histone modifications are known to modulate chromatin structure, thereby inducing reversible and hereditable transcriptional regulation of genes.[26] Aberrant histone modifications have been strongly associated with the pathogenesis of human diseases.[27] Lysine methylation of histones is one of the most characterized modifications to date,[26] however, its role in Treg biology is not completely understood. Accumulating evidence now suggests that Treg function relies on enhancer of zeste homolog 2 (EZH2), evident by the susceptibility of Treg-specific EZH2-deleted mice to multi-organ autoimmunity including colitis.[28,29] EZH2, the catalytic subunit of the polycomb repressive complex 2 (PRC2), is known to mediate the trimethylation of lysine 27 on histone 3 (H3K27me3), thereby facilitating chromatin remodeling and gene transcriptional repression.[30] EZH2 also is important for T-cell development and function.[31] Our recent work showed that up-regulation of FOXP3–EZH2 co-target genes was a unique feature of $CD4^+$ T cells isolated from the terminal ileum of Crohn's disease (CD) patients,[29] thus indicating a potential role for $FOXP3^+$ Treg dysfunction in disease pathogenesis. Indeed, genetic studies from families with early onset IBD or in combination with systemic autoimmunity have identified disease-causing missense mutations in anti-inflammatory *IL10*/*IL10R*[32,33] and *CTLA4*[34] genes, thus implying that intact Treg function potentially plays an important role in the suppression of human intestinal inflammation. Congruent with this notion, our previous work in a family with a missense variant in the sixth exon of the *FOXP3* gene (c.694A>C), which induced cysteine residue 232 to glycine mutation (FOXP3–C232G), was associated with impaired Treg function, intestinal inflammation, and a milder form of IPEX-like manifestations. This heritable FOXP3 mutation led to early onset IBD that was characterized by mucosal ulceration and severe inflammation in affected family members.[35] Despite this genetic linkage study, the molecular mechanism responsible for disease pathogenesis was unknown. Guided by our previous work showing aberrant expression of FOXP3–EZH2 co-target genes in adult human CD lesions, and the association of FOXP3–C232G variant to a monogenic form of IBD, we investigated the mechanisms that regulate the recruitment of FOXP3–EZH2 complexes to the chromatin in normal and disease states.

In this study, we postulated that the disruption of FOXP3–EZH2 protein interaction and consequent loss of co-repressive function of these proteins may contribute to human intestinal inflammation. By using clinically relevant and disease-inducing FOXP3 variants, we assessed the EZH2-binding capacity of FOXP3–C232 mutants and found that EZH2 interaction was abolished and consequently failed to efficiently repress relevant gene targets. Generalizing this observation, IL6-induced signals similarly disrupt FOXP3–EZH2 interaction in a manner reversible by Janus kinase (JAK) 1/2 inhibition. Interestingly, in lamina propria–derived $CD4^+$ T cells isolated from human CD biopsy specimens, we found a reduced presence of FOXP3–EZH2 protein complexes. Thus, our data support a model whereby loss of FOXP3–EZH2 protein interaction in Tregs via diverse mechanisms is an indication of a compromised Treg physiology that may perpetuate intestinal inflammation. These observations highlight the clinical importance and approaches for improving Treg function in the context of inflammation.

Results

FOXP3 Interacts With EZH2 in Murine-Induced Tregs and Freshly Isolated PBMC-Derived Human Tregs

In murine Tregs, FOXP3 gene targets overlap with EZH2-mediated H3K27me3-repressive peaks as shown by chromatin-immunoprecipitation (ChIP) sequencing analysis,[36] however, structural insight into the regulation of FOXP3–EZH2 protein interaction is lacking. To characterize this interaction, naive murine $CD4^+$ T cells isolated from the spleen were differentiated into Tregs (induced) or T helper (Th)17 cells in culture under specific polarizing conditions. These cells were subjected to an in situ proximity ligation assay (PLA) and co-immunoprecipitation (co-IP) (Figure 1) using specific antibodies against endogenous FOXP3 and EZH2. By using PLA, we visually and quantitatively monitored protein–protein interactions in close proximity (<30 nm) in individual cells at single-molecule resolution detectable via fluorescent signals (shown in red) that serve as surrogate markers (Figure 1*A*). PLA and confocal imaging of cells showed that the majority of Tregs co-stained with FOXP3 and EZH2 antibodies showed nuclear PLA signals (red signals) (Figure 1*B*, third row, and quantified in 1*C*, % PLA^+ cells) in contrast to single-antibody–stained cells, co-stained Th17, or activated undifferentiated $CD4^+$ T cells (Figure 1, fourth and fifth rows, respectively). Congruent with the PLA studies, EZH2 co-purified with immunoprecipitated FOXP3 in murine Tregs in contrast to activated undifferentiated $CD4^+$ T cells (Figure 1*D*). Similarly, in human Tregs ($CD4^+CD25^{++}FOXP3^+$ cells) freshly isolated from peripheral blood mononuclear cell (PBMC) donors, FOXP3 interacted with EZH2 (magenta signal) irrespective of anti-CD3/-CD28–induced T-cell–receptor activation (Figure 1*E* and *F*). As a control, $CD4^+CD25^-$ cells show diminished FOXP3–EZH2 interaction (Figure 1*E*, first row, and *F*). Taken together, our data show a constitutive interaction between FOXP3 and EZH2 in murine and human Tregs, suggesting that FOXP3 and EZH2 may form protein–protein complexes on their target loci to mediate gene repression.

FOXP3 Constitutively Interacts With the PRC2 Complex

To test the generalizable nature of our findings, we used a nonimmune cellular in vitro system devoid of T-cell–specific signaling pathways and putative activators. We ectopically co-expressed tagged (His, myc, DDK) plasmids encoding human FOXP3 and EZH2 proteins in HEK293T cells, and subsequently performed PLA and co-IP studies (Figure 2*A–F*). Cells co-expressing both His–FOXP3 and myc–EZH2 showed robust nuclear FOXP3–EZH2 interaction (green signal) (Figure 2*A*, fourth row, and *B*) in contrast to myc–EZH2– or His–FOXP3–expressing cells (Figure 2*A*, first and second rows, respectively, and *B*). This result was validated using a second EZH2 construct (Myc–DDK–EZH2)

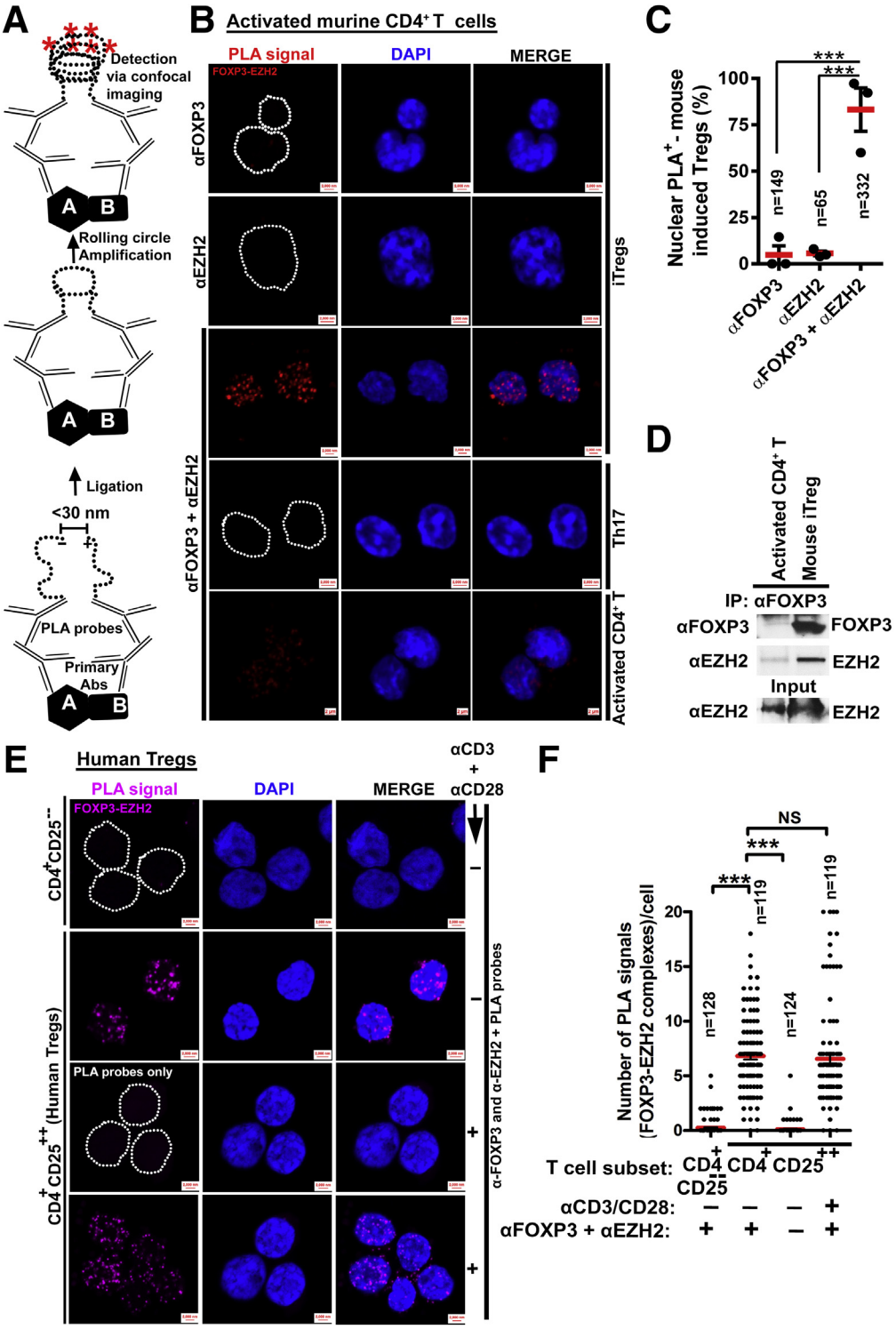

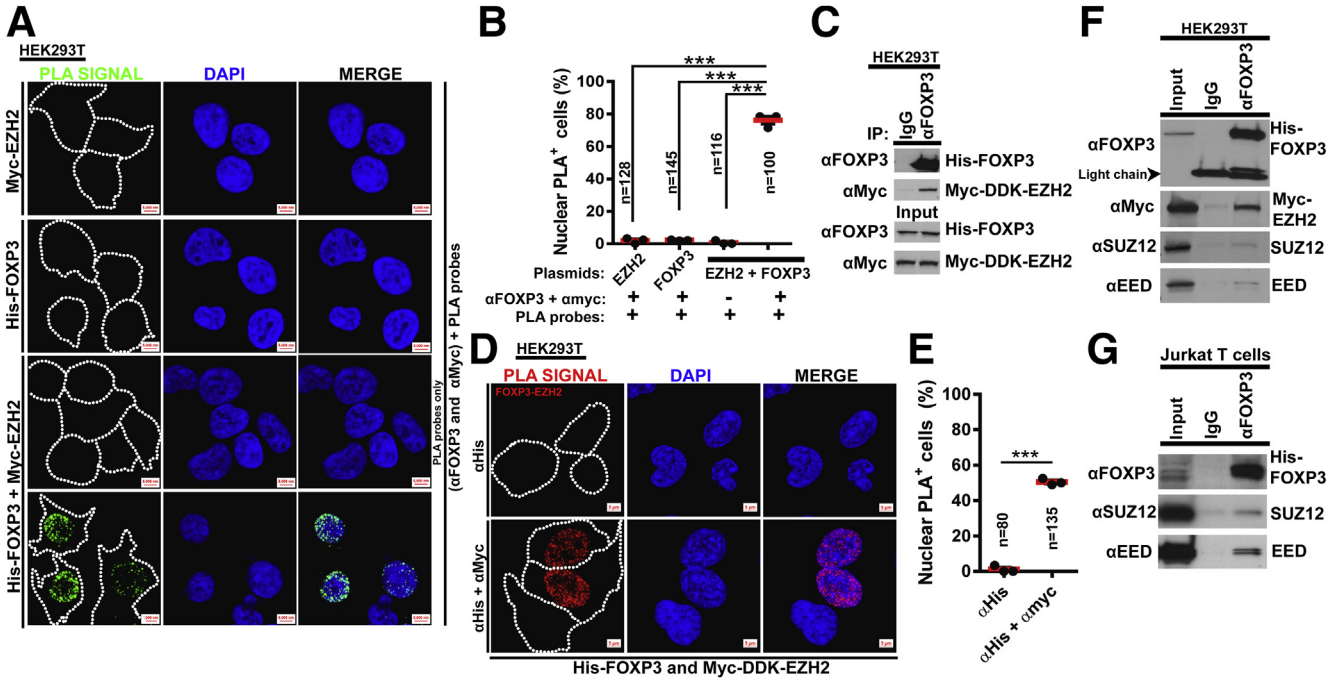

Figure 2. FOXP3 constitutively interacts with the PRC2 complex. HEK293T cells transfected with plasmids encoding either EZH2 (myc-tagged EZH2), FOXP3 (His-tagged FOXP3), or both for 48 hours were subjected to PLA or co-immunoprecipitation using the indicated primary antibodies. (*A*) Representative PLA images of cells from 3 independent experiments; first 3 rows are negative control experiments and green signals indicate a FOXP3–EZH2 interaction. *Scale bar*: 20 μm. (*B*) Quantitation of nuclear PLA signals in images from panel *A*; n = number of cells imaged. ***$P < .001$. *Red horizontal bars* indicate means ± SEM (1-way analysis of variance + Bonferroni test) from 3 independent experiments. (*C*) Whole-cell lysates from HEK293T cells transfected with plasmids encoding His–FOXP3 and myc–DDK–tagged EZH2 were subjected to immunoprecipitation with IgG or anti-FOXP3 antibody, immunoblotted for His–FOXP3 and myc–EZH2 with FOXP3 and myc antibodies. Input shows protein expression in whole-cell lysates. Data are representative of 3 independent experiments. (*D*) Cells from panel *C* were subjected to PLA using His antibody (negative control) or both His and myc antibodies. Red signals indicate FOXP3–EZH2 interaction; data are representative of 3 independent experiments. *Scale bar*: 20 μm. (*E*) Quantitation from 3 independent experiments of nuclear PLA signals in images from Figure 1*D*. ***$P < .001$. Red horizontal bars indicate means ± SEM (1-way analysis of variance + Bonferroni test). n = number of cells imaged. (*F* and *G*) Cell lysates from cell lines transfected with the indicated plasmids (FOXP3 and EZH2 in HEK293T cells or FOXP3 alone in Jurkat T cells) were subjected to immunoprecipitation with IgG or anti-FOXP3 antibody; immunoblotted for His–FOXP3, myc–EZH2, and the other PRC2 subunits SUZ12 and EED with the indicated antibodies. Data are representative of 3 independent experiments. DAPI, 4′,6-diamidino-2-phenylindole.

in co-IP (Figure 2*C*) and PLA (Figure 2*D* and *E*) assays. Consistent with a previous report,[36] ectopically expressed human FOXP3 constitutively interacted with endogenous suppressor of zeste (SUZ12), as well as previously uncharacterized embryonic ectoderm development (EED) in HEK293T and Jurkat T cells (Figure 2*F* and *G*). SUZ12 and EED are known to support the chromatin remodeling function of the enzyme EZH2. These multiparametric biochemical experiments suggest that FOXP3 constitutively forms a protein complex with the core subunits of PRC2.

Figure 1. (***See previous page***). **FOXP3 interacts with EZH2 in murine induced Tregs (iTreg) and freshly isolated PBMC-derived human Tregs.** (*A*) Sketch depicts PLA to detect and quantify protein–protein interactions [A] and [B] <30 nm in close proximity or protein modifications by combining ligation of detection probes with rolling-circle amplification. (*B*) Mouse naive $CD4^+$ T cells isolated from spleen differentiated into Tregs (induced) or Th17 cells followed by PLA. Representative confocal PLA images of $CD4^+$ T-cell subsets from 3 independent experiments show endogenous FOXP3–EZH2 protein interaction (red). (*C*) Quantification of PLA^+ cells from panel *B*. n = number of cells imaged. ***$P < .001$. *Red horizontal bar* shows means ± SEM from 3 independent experiments (1-way analysis of variance + Bonferroni test). (*D*) Whole-cell lysates from activated $CD4^+$ T cells or iTregs in panel *B* were subjected to immunoprecipitation with anti-FOXP3 and immunoblotted for FOXP3 and EZH2; input shows EZH2 protein expression in whole-cell lysates. Data are representative of 3 independent experiments. (*E*) Representative PLA images of PBMC-derived human Tregs ($CD4^+CD25^{++}$) from 3 healthy donors showing endogenous FOXP3–EZH2 interaction (magenta) before and after T-cell–receptor activation with antibodies against CD3 and CD28; $CD4^+CD25^-$ cells were used as negative controls. *Scale bar*: 5 μm. *Dotted white lines* denote the plasma membrane as seen on differential interference contrast images. Data are representative of 3 independent experiments. (*F*) Quantification of nuclear PLA signals (number of *dots* per cell) in images from *E*. n = number of cells imaged. ***$P < .001$; NS, non-significant *P* value. *Red horizontal bars* indicate means ± SEM (1-way analysis of variance + Bonferroni test) from 3 independent experiments. DAPI, 4′,6-diamidino-2-phenylindole.

Because the functional relevance of this complex has not been established in human pathophysiology, we next sought to characterize known disease-inducing FOXP3 mutations by their ability to complex with EZH2.

FOXP3 Cysteine 232 to Glycine (FOXP3–C232G) Mutation Implicated in Loss of Treg-Suppressor Function and Early Onset IBD Disrupts EZH2 Interaction and its Gene Co-repressor Function

We previously identified a novel private mutation in FOXP3 (C232G) leading to loss of Treg-suppressive capacity and severe familial IBD, a phenotype quite distinct from the IPEX clinical phenotype.[35] Although IPEX-inducing FOXP3 mutations, particularly in the leucine zipper (LZ) domain, have been characterized extensively,[37–39] no mechanistic information relevant to C232 and in close proximity to LZ IPEX mutations, particularly within the context of EZH2, exists. Thus, we subsequently investigated the impact of disease-associated FOXP3 LZ and C232 mutations on EZH2 recruitment and function (Figure 3*A*).

For this purpose, we studied the core promoter of the human *IL2* gene as a model system because the human *IL2* gene is known to be rapidly modified epigenetically upon T-cell activation.[40] We used an *IL2* luciferase construct containing 1.0 kb 5' flanking region of the human *IL2* gene cloned upstream of the luciferase gene. As anticipated, repression of phorbol 12-myristate 13-acetate (PMA)/ionomycin-induced *IL2* promoter activity by FOXP3 as measured by luciferase expression was reduced in the presence of the specific EZH2 inhibitor GSK126 (Figure 3*B*), thus confirming a critical role for EZH2 in our model system.

By using this well-characterized model system, we next investigated the repressive capacity of FOXP3 C232 mutation using FOXP3–LZ mutants as relevant controls. In support of previous reports,[37,41] IPEX-associated FOXP3–LZ mutants (L242P and K250Δ) poorly repressed the *IL2* promoter in contrast to wild-type (WT) FOXP3 (Figure 3*C*). Of note, the novel FOXP3 C232G mutant showed impaired *IL2*-repressive capacity similar to the FOXP3–LZ mutants (Figure 3*C*).

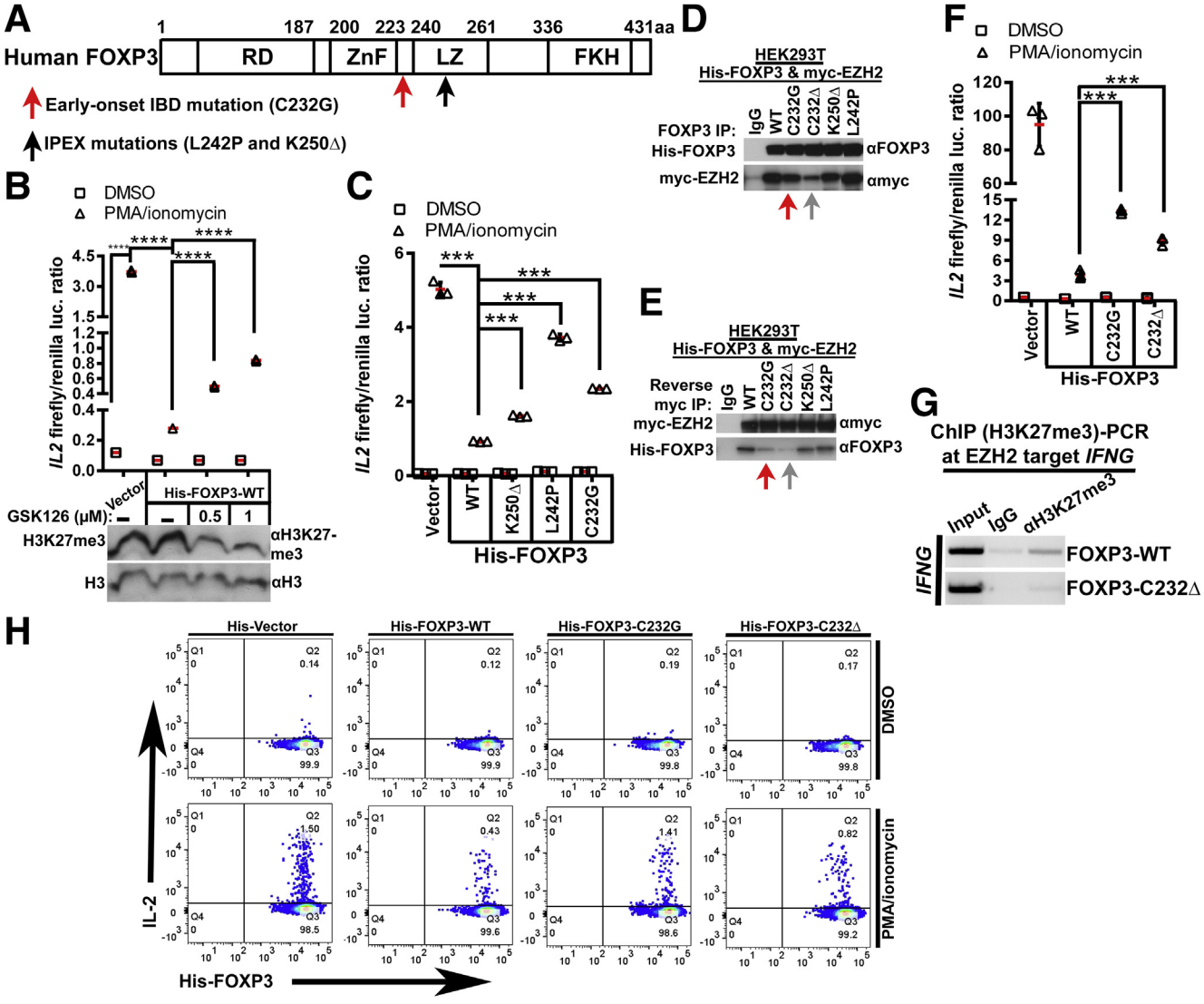

Subsequently, we assessed the ability of FOXP3–C232 mutants to co-immunoprecipitate with EZH2. Given that the mechanism of pathogenesis of LZ domain FOXP3 mutations is defined and not described to be EZH2-dependent,[37,38,42–44] these mutant constructs served as relevant controls. As shown by co-IP (Figure 3*D*) and reverse co-IP (Figure 3*E*), L242P and K250Δ retained EZH2 binding; however, both C232G and C232Δ mutants poorly associated with EZH2. These data suggest that C232 is critical for FOXP3–EZH2 interaction and potentially is necessary for FOXP3-mediated repressor function. We cannot completely rule out the possibility that residues within the FOXP3–LZ domain are similarly important for EZH2 recruitment.

To establish a mechanistic link between C232Δ-induced disruption of FOXP3–EZH2 interaction and EZH2-mediated gene silencing, we performed chromatin immunoprecipitation of the H3K27me3-repressive mark on the *IFNG* promoter locus, an IBD-relevant gene and an established FOXP3 target.[23] We initially evaluated the repressive function of the C232Δ mutant and confirmed that this mutant similarly displayed impaired repression of the *IL2* promoter (Figure 3*F*). In addition and comparable with the C232G mutant, the C232Δ mutant lacked the capacity to efficiently suppress PMA/ionomycin-induced IL2 cytokine production, as evident by increased frequency of $C232\Delta^{+}/IL2^{+}$-expressing cells in contrast to WT (Figure 3*H*, quadrant 2 [Q2], bottom row). We directly tested the ability of FOXP3–C232Δ mutant to recruit EZH2 to its target *IFNG* promoter by chromatin immunoprecipitation assay. As anticipated, C232 deletion within FOXP3 led to markedly diminished H3K27me3 at the *IFNG* promoter (Figure 3*G*). Thus, although IPEX-inducing FOXP3 mutations, particularly within the LZ domain, have been characterized extensively, we report a FOXP3 mutation that impairs protein association with EZH2.

IBD-Associated IL6-Induced Membrane-to-Nucleus Signaling Pathway Similarly Disrupts FOXP3–EZH2 Interaction in a Manner Reversible by JAK1/2 Inhibition

Thus far in our in vitro models, we have linked the pathogenesis of genetically induced IBD to destabilized FOXP3–EZH2 interaction, which is driven by FOXP3–C232 mutation. $FOXP3^{+}$ Tregs are known to respond to microenvironmental signals, and proinflammatory cytokines have been directly implicated in the pathogenesis of gastrointestinal inflammation.[45–49] Indeed, our recently published data set showed the IL6 signaling pathway to be one of the top up-regulated pathways in $CD4^{+}$ T cells from inflamed terminal ileum of a previous cohort of CD patients.[29] Thus, given the reported destabilizing effects of IL6 on Treg development and function,[50–52] we chose the IL6 signaling pathway as our model system for subsequent experiments. Acute IL6 treatment of PBMC-derived Tregs, in a time-dependent manner, disrupted FOXP3–EZH2 protein interaction (Figure 4*A*, third and fifth rows, and as quantitated in *B* and *C*) in contrast to vehicle-treated cells (Figure 4*A*, second row, and as quantitated in *B* and *C*). In addition, disruption of FOXP3–EZH2 interaction directly correlated with increasing concentration of IL6 (Figure 4*A*, third and seventh rows, and as quantitated in *B* and *C*). Flow cytometric analysis of cells confirmed that IL6 had no obvious

Figure 3. (***See previous page***). **FOXP3 cysteine 232 to glycine (FOXP3–C232G) mutation implicated in loss of Treg-suppressor function and early onset IBD disrupts EZH2 interaction and its gene co-repressor function.** (*A*) Schematic depicts structural domains within 50 kilodalton human FOXP3 (1–431 amino acids), detailing genetic mutations associated with IBD and IPEX syndrome. Structural domains include the following repressor domain (RD), zinc finger (ZnF), LZ, and forkhead (FKH)-DNA binding. *Red and black arrows* indicate amino acids mutated in IBD and IPEX patients. C232G, cysteine 232 to glycine; L242P, leucine 242 to proline; K250Δ, lysine 250 deletion. (*B*) Jurkat cells transfected with *IL2* firefly and renilla luciferase plasmids plus either empty vector or His–FOXP3 plasmids were treated with 0.4% dimethyl sulfoxide (DMSO)–vehicle control or indicated concentrations of EZH2 inhibitor GSK126. Thirty-six hours later, cells were treated with 0.4% DMSO–vehicle control or PMA/ionomycin for 12 hours to activate the *IL2* promoter as measured by firefly luciferase expression normalized to the renilla internal control. *Bottom panel*: Whole-cell lysates from transfected and GSK126-treated cells were immunoblotted for H3K27me3; the same membrane was stripped and reblotted for H3 as control. *Red horizontal bar* denotes the mean *IL2* firefly/renilla ratio ± SD from 3 replicates. $^{****}P < .0001$ (1-way analysis of variance + Bonferroni test). Result is representative of 3 independent experiments. (*C*) Jurkat cells expressing vector or FOXP3 (WT or mutants) plus luciferase plasmids were treated with DMSO or PMA/ionomycin as in panel *B*. *Red horizontal bar* denotes the mean *IL2* firefly/renilla ratio ± SD from 3 replicates. $^{***}P < .001$ (1-way analysis of variance + Bonferroni test). (*D* and *E*) Whole-cell lysates from HEK293T cells co-expressing myc-tagged EZH2 and His–FOXP3 WT or mutants were subjected to FOXP3 immunoprecipitation, immunoblotted for His–FOXP3 and myc–EZH2 using the indicated antibodies. *Red arrows* and *gray arrows* emphasize C232 mutants within FOXP3. Data shown are representative of 3 independent experiments. (*F*) Jurkat cells expressing empty vector or His–FOXP3 (WT or C232 mutants) and indicated luciferase plasmids were treated with 0.4% DMSO or PMA/ionomycin. *Red horizontal bar* denotes the mean *IL2* firefly/renilla ratio ± SD from 3 replicates; $^{***}P < .001$ (1-way analysis of variance + Bonferroni test). Result is representative of 3 independent experiments. (*G*) Chromatin from Jurkat cells expressing FOXP3–WT or –C232Δ were incubated with IgG control or anti-H3K27me3 antibody, polymerase chain reaction (PCR) for the *IFNγ* promoter was performed to assess the presence of H3K27me3 repressive mark. Data shown are representative of 3 independent experiments. (*H*) Jurkat cells overexpressing empty His-vector plasmid (control), His–FOXP3 WT or His–FOXP3 mutants (C232G and C232Δ) were treated with 0.2% DMSO (*top row*) or PMA/ionomycin (*bottom row*) for 12 hours. Cells were permeabilized and then stained with fluorescently conjugated IL2 and His antibodies against intracellular IL2 and His-tagged FOXP3. *Dot plot* in quadrant 2 (Q2) depicts the frequency, in percentage, of IL2 and His co-expressing cells as measured by flow cytometry. Data shown are representative of 3 independent experiments.

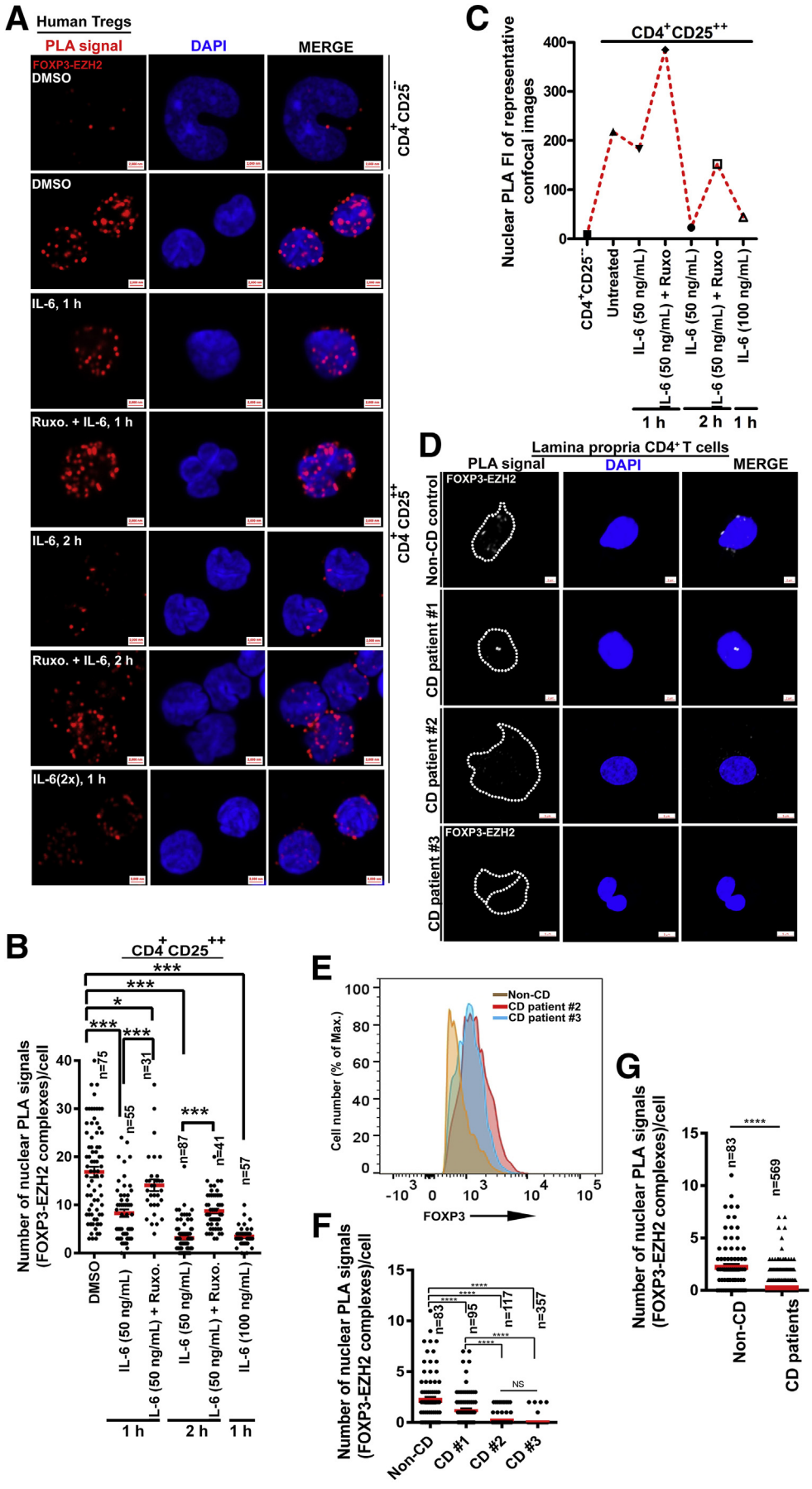
A
Human Tregs
PLA signal
DAPI
MERGE
FOXP3-EZH2
DMSO
DMSO
IL-6, 1 h
Ruxo. + IL-6, 1 h
IL-6, 2 h
Ruxo. + IL-6, 2 h
IL-6(2x), 1 h
CD4+CD25--
CD4+CD25++
B
CD4+CD25++
Number of nuclear PLA signals (FOXP3-EZH2 complexes)/cell
DMSO
IL-6 (50 ng/mL)
IL-6 (50 ng/mL) + Ruxo.
IL-6 (50 ng/mL)
IL-6 (50 ng/mL) + Ruxo.
IL-6 (100 ng/mL)
1 h
2 h
1 h
C
CD4+CD25++
Nuclear PLA FI of representative confocal images
CD4+CD25--
Untreated
IL-6 (50 ng/mL)
IL-6 (50 ng/mL) + Ruxo
IL-6 (50 ng/mL)
IL-6 (50 ng/mL) + Ruxo
IL-6 (100 ng/mL)
1 h
2 h
1 h
D
Lamina propria CD4+ T cells
PLA signal
DAPI
MERGE
FOXP3-EZH2
Non-CD control
CD patient #1
CD patient #2
CD patient #3
E
Non-CD
CD patient #2
CD patient #3
Cell number (% of Max.)
FOXP3
F
Number of nuclear PLA signals (FOXP3-EZH2 complexes)/cell
Non-CD
CD #1
CD #2
CD #3
NS
G
Number of nuclear PLA signals (FOXP3-EZH2 complexes)/cell
Non-CD
CD patients

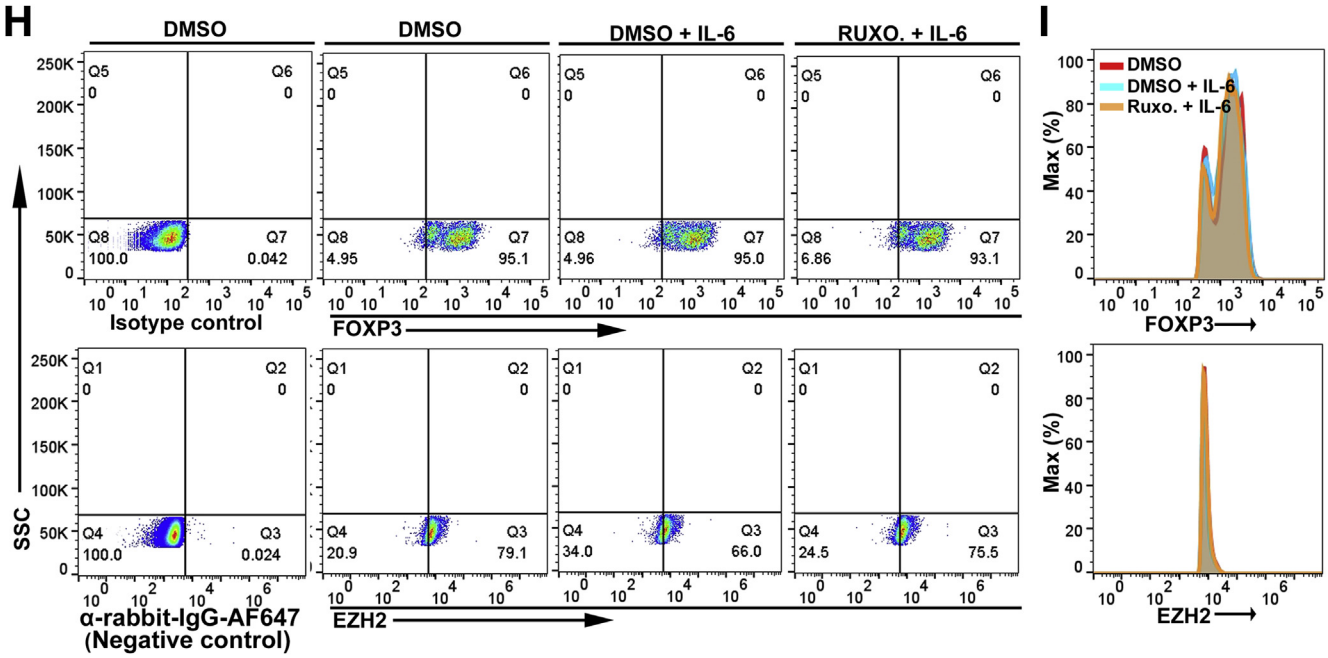

Figure 4. (*continued*).

effect on either FOXP3/EZH2 protein expression (Figure 4*I*) or the frequency of FOXP3$^+$ and EZH2$^+$ Tregs (Figure 4*H*). Given the clinical efficacy and interest in the use of small-molecule JAK inhibitors for the treatment of human immune-mediated diseases such as rheumatoid arthritis, IBD, and myelofibrosis,[53] we chose to further characterize the involvement of the IL6-dependent JAK–signal transducer and activator of transcription (STAT) pathway through tyrosine phosphorylation assays and ruxolitinib-mediated JAK1/2 inhibition. First, corroborating our data in primary cells, we validated the IL6-induced disruption of FOXP3–EZH2 interaction in HEK293T cells via co-IP (Figure 5*A* and *B*, lanes 2 compared with lanes 3). Interestingly, the effect of IL6 was dynamic, with the interaction restored at later time points potentially owing to a negative feedback mechanism (Figure 5*A* and *B*, lanes 4 and 5 compared with lanes 2). Primary Tregs then were treated with IL6 in the presence of the JAK1/2 inhibitor ruxolitinib, which prevented IL6-induced disruption of FOXP3–EZH2 complexes (Figure 4*A*, fourth and sixth rows, and as

Figure 4. (***See previous page***). **IBD-associated IL6-induced membrane-to-nucleus signaling pathway similarly disrupts FOXP3–EZH2 interaction in a manner reversible by JAK1/2 inhibition.** (*A*) Confocal microscopic PLA images shows endogenous FOXP3–EZH2 interaction (red signals) in the nucleus of CD4$^+$CD25^{++} cells (Tregs) before (0.2%–0.4% dimethyl sulfoxide [DMSO]), after IL6 (50 or 100 ng/mL, 2×) or after IL6 and JAK1/2 inhibitor ruxolitinib pretreatment (10 μmol/L). CD4$^+$CD25$^-$ cells were used as negative controls. *Scale bar*: 5 μm. Result is representative of 3 independent experiments using freshly isolated PBMC-derived Tregs from 3 different donors. (*B*) Quantitation of nuclear PLA signals in images from panel *A* (rows 2–7). n = number of cells imaged. ***$P < .001$, *$P < .05$. *Red horizontal bars* indicate means ± SEM (1-way analysis of variance + Bonferroni test) from 3 independent experiments. (*C*) Quantitation of red fluorescent intensities displayed by representative cells shown in panel *A*. Data are representative of 3 independent experiments. (*D*) Representative confocal microscopic PLA images of intestinal CD4$^+$ T cells from 3 CD patients showing reduced FOXP3–EZH2 complexes (white signals) in comparison with non-CD control cells. *Dotted white lines* denote the plasma membrane as seen on differential interference contrast images. *Scale bar*: 2–5 μm. Simple endoscopic scores for CD patients were as follows: patient 1, 18; patient 2 (on 30 mg of prednisone), 10; and patient 3 (on 8 mg of budesonide 1 time daily), 8. (*E*) Lamina propria CD4$^+$ T cells from panel *D* were stained with fluorescently conjugated FOXP3 antibody and subjected to flow cytometric analysis. Histogram overlay compares FOXP3 expression in isolated CD4$^+$ T cells (control vs CD patients 2 and 3). (*F*) Quantitation of nuclear PLA signals/CD4$^+$ T cells from individual CD patients (patients 1, 2, or 3) vs non-CD CD4$^+$ T cells. n = number of cells imaged. *Red horizontal bars* denote means ± SEM. ****$P < .001$; NS, 1-way analysis of variance + Bonferroni test. (*G*) Quantitation of nuclear PLA signals/CD4$^+$ T cells from all 3 CD patients vs non-CD control as shown in panel *F*. n = number of cells imaged. ****$P < .0001$. *Red horizontal bars* indicate means ± SEM (Student *t* test). (*H*) PBMC-derived human Tregs were treated with DMSO, IL6 (50 ng/mL), or IL6 (50 ng/mL) plus 10 μmol/L ruxolitinib (ruxo.) for 2 hours in serum-free media as in panel *A*, and then permeabilized and stained for FOXP3 or EZH2 with fluorochrome-conjugated antibody or primary antibody, respectively. *Dot plots* show the frequency, in percentage, of cells expressing FOXP3 (*top row*: quadrant 7 [Q7]) or EZH2 (*bottom row*: quadrant 3 [Q3]) as measured by flow cytometric analysis. For negative controls, IgG isotype or fluorescently conjugated secondary antibody were used to stain cells. (*I*) Histograms depict FOXP3 or EZH2 expression in cells from panel *H*. Data are representative of 3 independent experiments. DAPI, 4′,6-diamidino-2-phenylindole; FI, fluorescent intensity; SSC, side scatter.

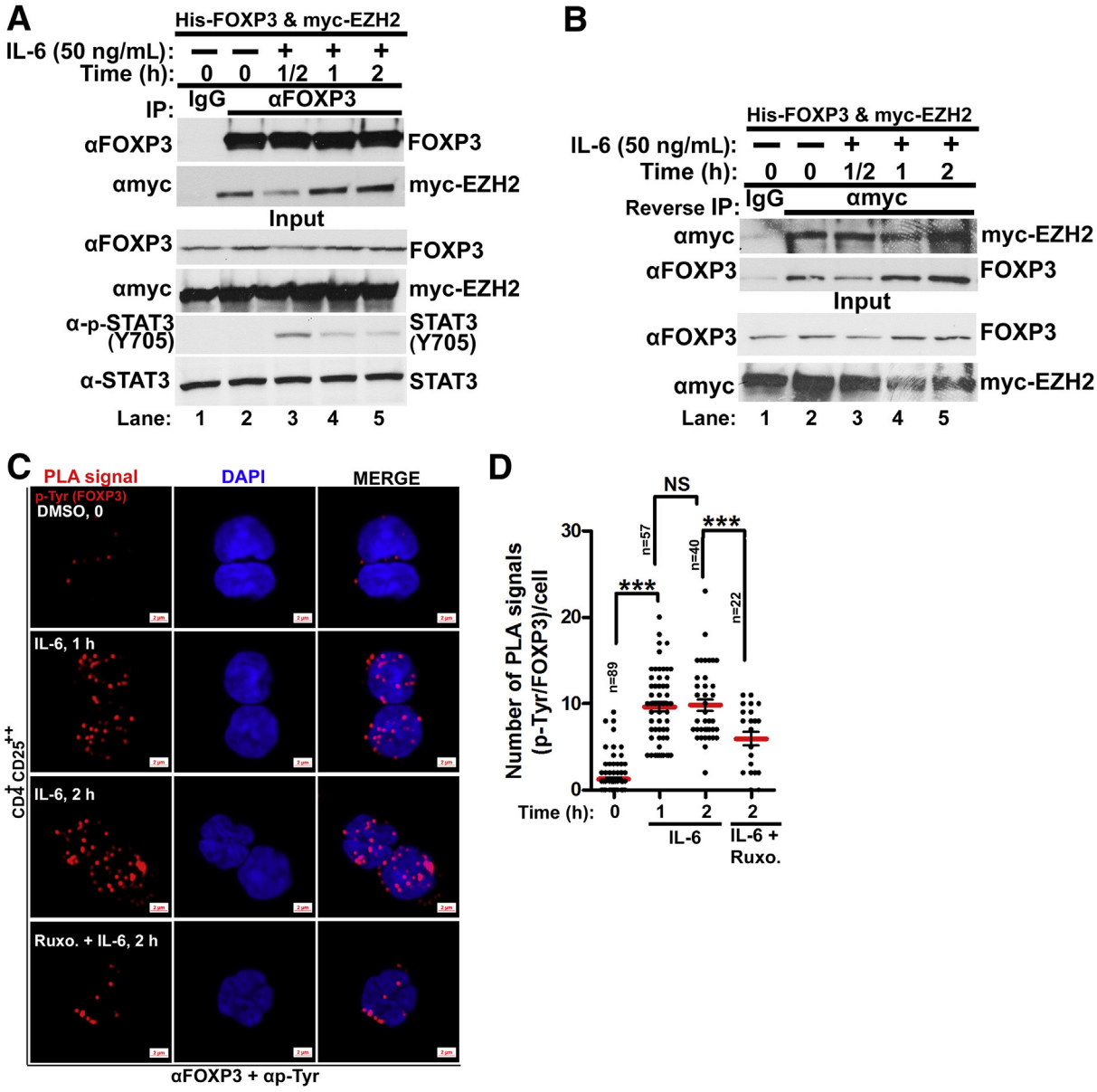

Figure 5. IL6-induced disruption of FOXP3–EZH2 protein interaction correlates with increased STAT3 activation and FOXP3 tyrosine phosphorylation. (*A*) HEK293T cells ectopically expressing plasmids encoding His–FOXP3 and myc–EZH2 were treated with IL6 (50 ng/mL) for the indicated duration under reduced-serum conditions. Whole-cell lysates were subjected to immunoprecipitation with IgG or FOXP3 antibody and immunoblotted for His–FOXP3. The same membrane was stripped and reblotted for myc–EZH2. For input, lysates were immunoblotted for His–FOXP3, myc–EZH2, STAT3, and p-STAT3 (Y705) with their corresponding antibodies. (*B*) Reverse co-immunoprecipitation of experiment in panel *A* using myc antibody for EZH2. Data are representative of 3 independent experiments. (*C*) Representative confocal PLA images of human $CD4^{+}CD25^{++}$ cells (Tregs) shows tyrosine phosphorylated FOXP3 (red) in response to IL6 (50 ng/mL) alone or in combination with ruxolitinib (Ruxo.) (10 μmol/L) for the indicated time points. To detect FOXP3 tyrosine phosphorylation, cells were stained with pan p-Tyr antibody and specific FOXP3 antibody as indicated. Data are representative of 3 independent experiments. *Scale bar*: 2 μm. (*D*) Quantitation of nuclear PLA signals in images from panel *C*. n = number of cells imaged. ***$P < .001$; NS, non-significant *P* value. *Red horizontal bars* indicate means ± SEM (1-way analysis of variance + Bonferroni test) from 3 independent experiments using cells from PBMC donors. (*E* and *F*) PBMC-derived human Tregs were treated with IL6 or both IL6 and JAK1/2 inhibitor ruxolitinib for the indicated time points. PLA and confocal microscopic imaging were performed to detect and visualize phosphorylated (p) residues (p-Y705 and p-S727) on STAT3 (red signals) by staining cells with the indicated antibodies. Representative images from 3 independent experiments are shown from 3 different donors. *White dotted lines* mark the cytoplasm of cells while 4′,6-diamidino-2-phenylindole (DAPI) stains the nuclei blue. Red PLA signals indicate phosphorylated tyrosine residue (Y) 705 on STAT3 in cells stained with both STAT3 and p-STAT3-Y705 antibodies or phosphorylated serine residue (S) 727 on STAT3 in cells stained with both STAT3 and p-STAT3-S727 antibodies. *Scale bar*: 5 μm. (*G* and *H*) Quantitation of nuclear PLA signals from images in panels *E* and *F*, respectively. n = number of cells imaged. *Red horizontal bars* denote means ± SEM. **$P < .01$ and ***$P < .001$ (1-way analysis of variance + Bonferroni test) from 3 independent experiments across 3 different donors.

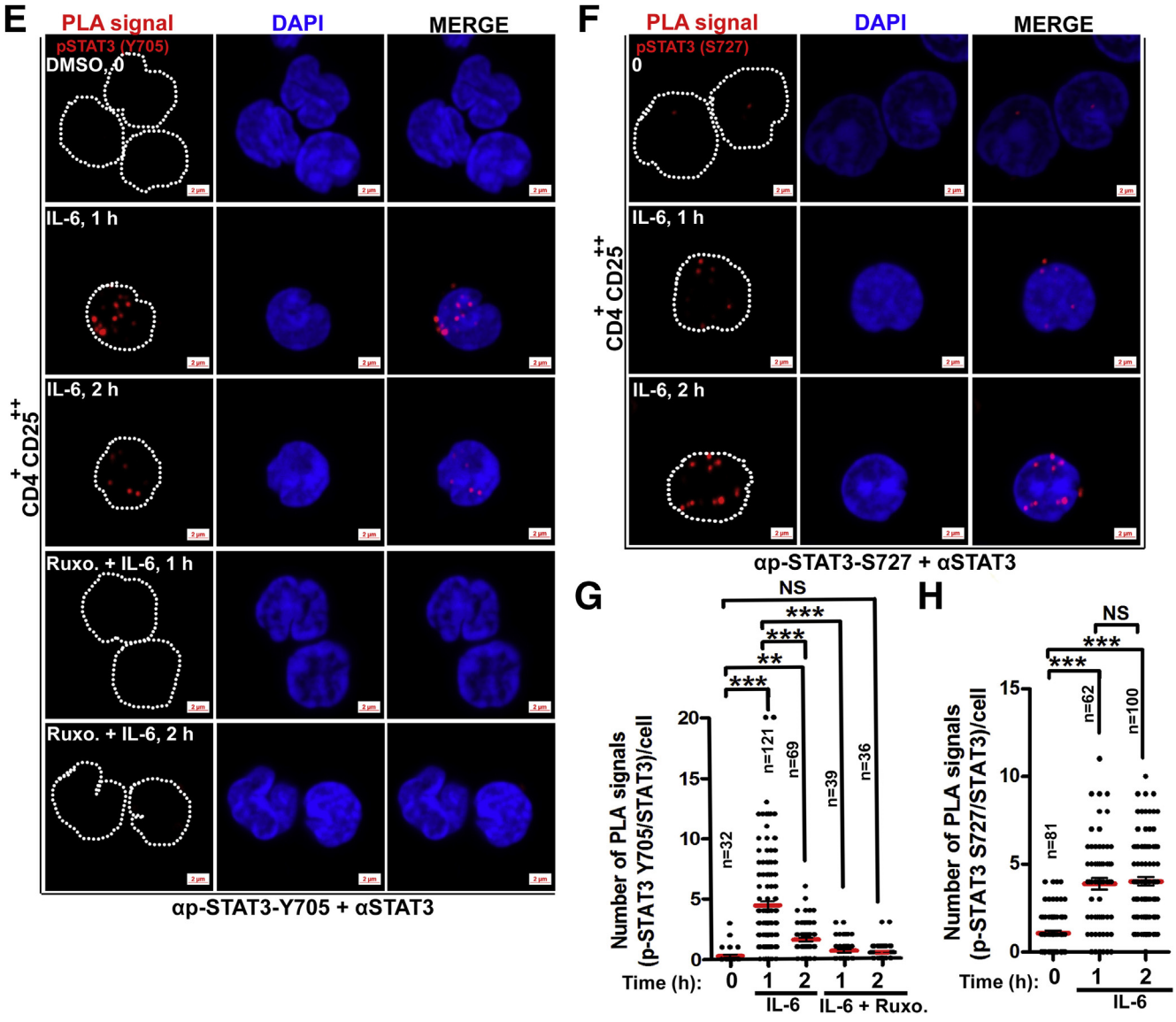

Figure 5. (*continued*).

quantitated in *B* and *C*). The demonstrated loss of FOXP3–EZH2 interaction correlated with increased tyrosine phosphorylation of FOXP3 (Figure 5*C*, as quantitated in *D*), and increased STAT3 activation (Figure 5*A*, lane 3, and *E*–*H*). Thus, using healthy donor Tregs, our data suggest that IL6-induced activation of JAK1/2 destabilizes FOXP3–EZH2 interaction.

Finally, we studied FOXP3$^+$ cells isolated from the intestinal lesions of human CD, a pathologic condition we previously identified to be associated with dysregulated EZH2-dependent FOXP3 transcriptional gene networks.[29] Specifically, we investigated whether the disruption of the FOXP3–EZH2 protein complex is a molecular feature of human CD via PLA using freshly isolated CD4$^+$ T cells from patient biopsy specimens. Inflamed colonic biopsy specimens were taken during endoscopy from 3 patients (patients 1, 2, and 3) diagnosed with severe to moderate CD based on simple endoscopic scoring for CD of 18, 10, and 8, respectively, as previously reported as a reliable assessment for disease severity.[54] Consistent with our hypothesis, CD CD4$^+$ T cells showed reduced FOXP3 and EZH2 protein interaction (white signals) in contrast to that of healthy controls (Figure 4*D*) as quantitated in Figure 4*F* and *G*. As relevant controls, total FOXP3 expression was comparable in non-CD and CD CD4$^+$ T cells (Figure 4*E*). Collectively, these observations suggest that the CD-associated inflammatory milieu potentially disrupts the constitutive binding of FOXP3 to EZH2 in Tregs. This consequently may impair Treg function in vivo, thereby perpetuating intestinal inflammation. Taken together with the JAK1/2 inhibition studies, our data suggest that this disease-relevant biochemical process potentially can be reversed by currently available JAK1/2 inhibitor therapy.

In summary, based on our study, we infer a mechanistic model explaining the pathobiological mechanisms that can be responsible for Treg abnormality. According to this

model, the physical interaction between FOXP3 and EZH2 necessary for gene co-repressive function can be attenuated by IBD-associated FOXP3-C232 mutation, resulting in impaired repression of target genes. Guided by this observation, we showed the generalizability of this paradigm to sporadic forms of human IBD evident by the diminished presence of FOXP3–EZH2 protein complexes in CD-associated $CD4^+$ T cells. Consistent with this paradigm, in human Tregs, IL6 signaling disrupted FOXP3–EZH2 protein interaction in a manner reversible by the JAK1/2 inhibitor ruxolitinib. Thus, we discovered a perturbed EZH2 pathway in Tregs as a clinically important epigenetic mechanism that is potentially responsible for Treg dysfunction during IBD progression.

Discussion

In a murine model, we previously showed that EZH2 expression in Tregs plays an important co-regulatory role in enforcing the immunosuppressive functions of FOXP3.[29] However, clinical evidence linking aberrant EZH2 function to intestinal inflammation and the mechanisms involved had remained elusive. Based on our previous work, the distinct presentation of the severe familial IBD, which was induced by FOXP3–C232G–mediated Treg dysfunction, led us to postulate a novel role for Treg-specific FOXP3–EZH2 interaction in suppressing gastrointestinal inflammation. By using this IBD-related private mutation to illuminate a more generalizable mechanism relevant to IBD pathophysiology, we then studied the impact of inflammatory signaling pathways on FOXP3–EZH2 protein interaction. This report contributed 2 major advances to the current state of understanding the functional relationship between FOXP3 and EZH2. First, we have now uncovered a novel pathobiological mechanism caused by loss of FOXP3 protein interaction with its obligatory co-factor EZH2 in the context of a genetic FOXP3–C232G mutation previously associated with early onset human IBD. Second, generalizing this observation, we show that CD lesion–derived lamina propria $CD4^+$ T cells isolated from patients show reduced FOXP3–EZH2 interaction. In primary human Tregs, the proinflammatory cytokine IL6 abrogates FOXP3–EZH2 interaction in a manner that correlates with increased post-translational modification of FOXP3. Exploring the mechanism, we showed that IL6-induced effects were reversible by inhibition of JAK1/2 activity. Collectively, our study advances insight into EZH2-mediated epigenetic function in Tregs and its involvement in human IBD pathophysiology. Our data show the immune-suppressive function of the FOXP3–EZH2 protein complex and highlights the therapeutic implication of stabilizing this interaction to improve Treg function during inflammation.

Numerous studies have intensely explored mechanisms of IPEX pathogenesis by structurally and functionally characterizing the consequences of disease-inducing FOXP3 mutations,[37–39] however, the mechanistic detail of how a rare FOXP3–C232G mutation is linked to IBD had remained uncharacterized. Driven by this fundamental gap in knowledge, we sought to study the molecular mechanism of pathogenesis of this rare human mutation in the context of EZH2 function. In this study, via biochemical and functional approaches, we established a physical and functional interaction between FOXP3 and EZH2. To structurally characterize mechanisms that mediate this constitutive physical interaction as well as its clinical relevance, we used naturally occurring and disease-causing FOXP3 mutations associated with IPEX and IBD to identify residues required for EZH2 binding. IBD-associated FOXP3–C232G and FOXP3–C232Δ mutations impaired FOXP3's ability to bind EZH2 and therefore caused deficiencies in the repression of *IL2*. Moreover, the H3K27me3-repressive mark on the EZH2 target gene *IFNG* was reduced in the chromatin of cells isolated from FOXP3–C232Δ–expressing cells compared with that of wild-type FOXP3, which is indicative of EZH2 dysfunction. Our study is consistent with the paradigm of how molecular mechanisms of disease pathogenesis can be driven by genetic mutations or nongenetic events. For example, basic zipper transcription factor–regulon, which we previously found to be differentially expressed in CD lesion–derived $CD4^+$T cells,[29] recently was reported to be associated with an IPEX-inducing FOXP3-A384T mutation evident from loss of basic zipper transcription factor expression and function.[55]

Although adoptive transfer studies in animal models of colitis have shown a critical role for Tregs in suppressing chronic intestinal inflammation,[56–58] the observation that ex vivo cultured human Tregs isolated from colonic mucosa of CD patients showed normal functional properties in vitro have remained thought-provoking.[59–61] This discrepancy has been attributed to the ex vivo culturing conditions in which human Tregs were expanded before conducting in vitro functional assays. Here, we report that human CD lesion–derived lamina propria $CD4^+$ T cells show minimal FOXP3–EZH2 protein interaction in contrast to non-CD control cells. This is consistent with our previously described observation that gene networks co-regulated by FOXP3 and EZH2 were up-regulated in intestinal lesion $CD4^+$ T cells from CD patients.[29] In addition, these CD $CD4^+$ T cells showed a marked Th1/Th17 effector-like phenotype in a fashion similar to murine EZH2-deleted $FOXP3^+$ Tregs cultured ex vivo.[29] Indeed, an increase of proinflammatory cytokines, such as IL6, is a hallmark of human IBD. In murine models of autoimmune diseases, IL6 favors Th17 cell differentiation and function while opposing Treg differentiation.[50,62] For example, IL6-unresponsive antigen-specific Tregs obtained via T-cell–conditional deletion of IL6R signaling subunit glycoprotein 130 showed improved protection against IL17-mediated experimental autoimmune encephalomyelitis while Treg depletion re-established the disease. Although other studies in murine cells have additionally linked the mechanism of IL6-induced inhibition of Treg function to attenuated FOXP3 protein expression,[63] we have shown the applicability of our findings broadly to IBD pathogenesis by revealing that acute treatment of Tregs with IL6 impaired FOXP3–EZH2 protein interaction. This incomplete attenuation of FOXP3–EZH2 interaction by IL6

suggests that additional proinflammatory signals, such as tumor necrosis factor-α) and IL21, as well as genetic aberrations, potentially are required for the maximum disruption of this interaction. For example, tumor necrosis factor-α–induced FOXP3 serine dephosphorylation has been associated with rheumatoid arthritis pathogenesis.[64] In line with the idea that FOXP3–EZH2 interaction is potentially regulated by post-translational modifications, IL6 signals had no effect on the FOXP3/EZH2 protein levels but rather augmented FOXP3 tyrosine phosphorylation. Therefore, identifying cytokine-induced posttranslational modifications on FOXP3 and EZH2, and how it impacts FOXP3–EZH2 interaction and Treg function in vivo, merits further investigation. In addition, the impact of proinflammatory cytokine signaling on other transcription factors, such as T-box protein 21, which is important for Treg stability and function, will be relevant.[65] Our work suggests that Tregs deficient in optimal FOXP3–EZH2 protein interaction potentially contribute to IBD pathogenesis. In addition, because IBD is characterized by cytokine imbalance, characterizing the Treg-suppressive capacity in vitro under inflammatory conditions that closely resemble those observed human IBD will be more relevant. Our data suggest that IL6-induced signaling events potentially can dampen Treg function at the level of FOXP3–EZH2 protein complexes; therefore, rendering Tregs insensitive to the effects of IL6 during IBD progression may curb disease severity.

The use of anti-IL6/IL6R therapies have led to clinical responses in cohorts of CD patients,[66] however, off-target effects of inhibiting this pleiotropic cytokine have slowed further clinical development in IBD. To minimize unwanted side effects that may arise from direct IL6/IL6R blockade, the need to identify targetable downstream mediators of IL6 signals is imperative. In our study, we associated reduced FOXP3–EZH2 protein complexes in CD $CD4^+$ T cells, a phenomenon mimicked by Tregs upon exposure to IL6 in a manner that was reversed by the JAK1/2 inhibitor ruxolitinib. Ruxolitinib, an adenosine triphosphate–competitive inhibitor of JAK1/2, is Food and Drug Administration–approved for the treatment of myeloproliferative disorders, whereas other JAK inhibitors currently are being therapeutically explored for IBD treatment.

In conclusion, our findings highlight the importance of FOXP3–EZH2 protein interaction in gene-silencing function. This interaction is clinically relevant in the context of genetic FOXP3 alteration that consequently abrogates EZH2 binding and its co-repressive capability. Similarly, proinflammatory cytokine signals can impair FOXP3–EZH2 protein interaction potentially through posttranslational modifications that can serve as biomarkers for Treg dysfunction and clinical response to biologics in IBD, as well as other autoimmune diseases and inflammatory conditions. These findings may guide novel efforts to develop safe therapies or approaches for desensitizing Tregs from the damaging effects of proinflammatory signals. Our study indicates potential therapeutic approaches and mechanisms for improving Treg function during IBD pathogenesis via stabilizing FOXP3–EZH2 interaction.

Materials and Methods

Human Biopsy Specimens

De-identified biopsy specimens from inflamed colonic mucosa were obtained from 3 CD patients diagnosed by established clinical, radiologic, and histopathologic criteria (2 men, ages 27 [patient 1] and 35 [patient 2] years, and 1 woman, age 54 years [patient 3]). For comparison, biopsy specimens were obtained from healthy controls (1 man and 1 woman, both ages 59). CD patient 1 had a severe level of inflammation in affected areas and was not on anti-inflammatory steroid medications whereas CD patients 2 and 3 showed moderate levels of inflammation and were on steroidal medications at the time (30 mg of prednisone, and 8 mg of budesonide 1 time/d, respectively) when biopsy specimens were taken. The study was approved by the Institutional Review Board committee-approved protocol (13-000712) and written informed consent was received from participants before inclusion in this study.

Animal Work and Ethics

C57BL/6J mice were initially purchased from the Jackson Laboratory and bred in convectional housing in the Mayo Clinic animal facility. All mice used in the experiments were males 5–10 weeks of age. Animal work was performed in accordance with reviewed and approved protocols by the Mayo Clinic Institutional Animal Care and Use Committee.

Isolation and Culture of $CD4^+$ T Cells From Colonic Biopsy Specimens

Tissue biopsy specimens from each individual were rinsed in 0.9% NaCl and then placed in 1 mmol/L EDTA Duchmann media (RPMI 1640 supplemented with 10% fetal calf serum [FCS], 1% penicillin/streptomycin, 1% gentamicin sulfate, 10 mmol/L HEPES, and β-mercaptoethanol) for 15 minutes in a 37°C CO_2 incubator to remove epithelial cells. Biopsy specimens were digested in a 37°C CO_2 incubator with a cocktail of enzymes containing 1 mg/mL each of collagenase, DNase, and trypsin inhibitor for 1–2 hours. Digested tissue was filtered through a 70-μm cell strainer to obtain single cells, centrifuged at 1200 rpm for 10 minutes. The pellet was suspended in commercially available beads for human $CD4^+$ T cell isolation according to the manufacturer's instructions (cat. 130-096-533; lot 5180406200; Miltenyi Biotec, San Diego, CA). Isolated $CD4^+$ T cells subsequently were subjected to in situ PLA and fluorescence-activated cell sorting.

Isolation of Tregs From Human PBMCs

The $CD4^+CD25^{++}$ regulatory T-cell isolation kit (cat. 130-091-301, lot 5180316290; Miltenyi Biotec) was used for isolating Tregs from human PBMCs according to the manufacturer's instructions. Briefly, a specified volume of isolated platelet was diluted in phosphate-buffered saline (PBS) and then added to Ficoll Paque Plus (Pittsburgh, PA). This mixture then was centrifuged at 1500 rpm for

30 minutes at 12°C in a swinging bucket rotor without brakes. The lymphocyte layer was removed and washed with PBS followed by centrifugation at 1200 rpm for 10 minutes at 12°C. Lysis buffer was added to the cells, incubated for 5 minutes at room temperature, and spun down at 800 rpm for 10 minutes to remove platelets. Lymphocytes were suspended in RPMI + 10% FCS (Gibco, Carlsbad, CA) for 30 minutes to obtain the desired nonadherent lymphocytes. These freshly prepared nonadherent lymphocytes or PBMCs then were subjected to $CD4^{+}CD25^{++}$ Treg isolation to obtain super pure Tregs. Isolated $CD4^{+}CD25^{-}$ were kept and used as negative controls in relevant experiments as indicated.

Cells, Cell Culture, Differentiation of $CD4^{+}$ T Cells, Stimulation Conditions, and Statistical Analysis

Jurkat T cells were maintained in medium A (RPMI 1640 supplemented with 10% FCS, 10 mmol/L HEPES, pH 7.4, and 2 mmol/L L-glutamine) at less than 10^{6} cells/mL. HEK293T cells were maintained in medium supplemented with 10% FCS, 4.5 g/L D-glucose, and L-glutamine. Jurkat cells were activated with plate-bound anti-human CD3 (5 μg/mL, clone OKT3, cat. 16-0037-85, lot 7347573; Affymetrix eBioscience, Santa Clara, CA) and anti-human CD28 (2 μg/mL, clone CD28.2, cat. 555735, lot 7340520; BD Biosciences, San Jose, CA) or cell activation cocktail (cat. 423302, lot B248900; BioLegend, San Diego, CA) containing 0.081 μmol/L PMA and 1.34 μmol/L ionomycin. Naive $CD4^{+}$ T cells were isolated from mice spleen using the $CD4^{+}$ T-cell isolation kit according to the manufacturer's instructions (cat. 130-104-454, lot 5171103089; Miltenyi Biotec). For PLA studies, Th17 cells were obtained by culturing $CD4^{+}$ T cells for 3 days in the presence of anti-mouse CD3 (2 μg/mL, clone 145-2C11, cat. 553057, lot 7241732; BD Biosciences), anti-mouse CD28 (2 μg/mL, clone 37.51, cat. 553294, lot 7068910; BD Biosciences), recombinant murine IL6 (50 ng/mL, cat. 216-16, lot 111450I2916; Peprotech, Rocky Hill, NJ), recombinant human transforming growth factor-β1 (1 ng/mL, cat. 100-21C, lot 0915354; Peprotech), anti-mouse IL4 (10 μg/mL, cat. 504108, lot B201326; BioLegend), anti-mouse interferon-γ (10 μg/mL, cat. 505812, lot B213311; BioLegend), and IL23 (5 μg/mL, cat. 1887-ML-010, lot MLE2613091; R&D Systems, Minneapolis, MN). Mouse-induced Tregs were obtained by culturing naive $CD4^{+}$ T cells for 3 days in the presence of anti-mouse CD3 (2 μg/mL), anti-mouse CD28 (2 μg/mL), human IL2 (100 U/mL; Peprotech), and transforming growth factor-β1 (5 ng/mL); naive mouse $CD4^{+}$ T cells expanded for 3 days in the presence of anti-CD3 (2 μg/mL), anti-mouse CD28 (2 μg/mL), and human IL2 (100 U/mL; Peprotech). Primary human Tregs were cultured overnight with anti-human CD3 (10 μg/mL, clone UCHT1, cat. 555329, lot 7347573; BD Biosciences), human IL2 (100 U/mL, Peprotech), and anti-human CD28 (2 μg/mL, clone CD28.2, cat. 555725, lot 8060981; BD Biosciences). Human Tregs were treated with human IL6 (50 ng/mL, cat. 200-06, lot 071316; Peprotech) and dimethyl sulfoxide or the JAK1/2 inhibitor ruxolitinib (cat. S1378; Selleckchem, Houston, TX) for the indicated time points.

Statistical Analysis

Data are expressed as the means ± SEM or ± SD as indicated. Differences between groups were compared using 1-way analysis of variance followed by the Bonferroni post hoc test in which $P < .05$ was the minimum requirement for a statistically significant difference using GraphPad Prism 5.0 software (San Diego, CA). Differences between 2 groups were compared using the Student t test.

PLA and Confocal Microscopy of Fixed Cells

The proximity ligation method relies on dual proximal binding by pairs of detection probes to protein molecules to generate amplifiable DNA strands. The oligonucleotides on the probes, when brought in close proximity of <30 nm by adjacent proteins, are enzymatically ligated to generate circularized DNA bound to the probe-antibody/protein complex. The circularized DNA then is amplified with one of the oligonucleotides serving as the primer. Fluorescently labeled product covalently linked to the antibody–protein complex then was imaged by confocal microscopy. To begin, cells were harvested and plated on 8-well Lab-Tek chamber slides (Thermo Fisher Scientific, Waltham, MA) coated with fibronectin (Corning, Corning, NY) for 3 hours to allow cell attachment, and then treated as indicated. Cells then were fixed with 4% paraformaldehyde, permeabilized with 0.15% Triton X-100 (Invitrogen, Carlsbad, CA), and then washed with PBS. Cells were blocked for 1 hour with 5% bovine serum albumin containing 0.1% glycine and then incubated with the indicated primary antibodies. Protein–protein interactions and post-translational modifications were measured by Duolink (Sigma, St. Louis, MO) in situ fluorescence PLA probes (cat. DUO92004, lot SLBV2508; cat. DUO92002, lot SLBT9623; cat. DUO92006, lot SLBT4800) and detection reagents (cat. DUO92008, lot SLBV3043) in accordance with the manufacturer's instructions. Cells were mounted with Duolink 4′,6-diamidino-2-phenylindole–containing mounting medium (cat. 82040, lot A61722/1; Sigma-Aldrich). Images of cells were captured by using a C-Apochromat 40× objective/1.20 W korrM27 of a fluorescent confocal microscope (LSM 780 AxioObserver; Carl Zeiss, Jena, Germany). Images were processed using the Zen lite 2012 software (Carl Zeiss). Quantitation of nuclear PLA signals from cell images were performed as follows: percentage of cells positive for nuclear PLA dots, number of nuclear PLA signals per cell, or nuclear PLA fluorescent intensity. To quantitate the percentage of cells positive for PLA signals, cells that displayed no PLA dot were considered to be negative and those with more than 1 PLA dot were considered PLA positive and then expressed as a percentage of total cells that were imaged. To quantitate the number of PLA signals per cell, the number of PLA dots per cell was counted. To quantitate PLA fluorescent intensity, a line was drawn around the nuclei and fluorescence values were generated using ImageJ (National Institute of Health, Bethesda, MD) and plotted using Prism (GraphPad Software, San Diego, CA).

Antibodies for PLA

Primary antibodies used were rabbit monoclonal anti-FOXP3 (1:500, cat. ab54501, lot GR285227-2; Abcam, Cambridge, MA), mouse monoclonal anti-EZH2 (1:100, cat. 3147; Cell Signaling, Beverly, MA), mouse monoclonal anti-myc (1:500, cat. 2276, lot 24; Cell Signaling), rabbit monoclonal anti-His (1:500, cat. sc-499, lot 11214; Santa Cruz Biotechnology, Santa Cruz, CA), mouse monoclonal anti-phospho (p)-tyrosine (1:100, cat. sc-7020, lot L2916; Santa Cruz Biotechnology), mouse monoclonal anti-STAT3 (1:1000, cat. 9139, lot 7; Cell Signaling), rabbit monoclonal anti-pSTAT3-Y705 (1:100, cat. 9131, lot 30; Cell Signaling), rabbit monoclonal anti-pSTAT3-S727 (1:100, cat. 9134, lot 20; Cell Signaling).

Transient Transfections

Jurkat T cells were transiently transfected with indicated plasmids by electroporation at 315 mV for 10 ms and harvested 36–48 hours later. HEK293T cells were transiently transfected by Lipofectamine 2000 according to the manufacturer's instructions (cat. 11668-19, lot 1924211; Invitrogen, Carlsbad, CA) for 48–72 hours.

Co-IP Assay and Immunoblotting Analysis

HEK293T cells treated with human IL6 (50 ng/mL, cat. 200-06, lot 071316; Peprotech) and naive/differentiated $CD4^+$ T cells were harvested, washed with cold PBS, and lysed with RIPA lysis buffer containing 50 mmol/L Tris-HCL, pH 7.4, 1% NP-40, 150 mmol/L NaCl, and 2 mmol/L EDTA. Lysates were precleared with protein A (cat. 1134515001, lot 01001330; Roche, Indianapolis, IN) or protein G (cat. 11243233001, lot 10232222; Roche) beads for 1 hour and spun down. Supernatant was incubated with protein A or G beads plus the indicated primary antibody to immunoprecipitate the protein of interest. Co-immunoprecipitated and immunoprecipitated proteins were detected by Western blot using the indicated primary antibodies and horseradish-peroxidase–conjugated secondary antibodies.

Antibodies for Immunoblotting Analysis

Primary antibodies used were rabbit monoclonal anti-FOXP3 (3 ug/mL, cat. A301-900A; Bethyl Laboratories, Montgomery, TX), rat monoclonal anti-FOXP3 (2 ug/mL, cat. 14-4776-82, lot 4325553; eBioscience), rabbit monoclonal anti-EZH2 (1:1000, cat. 5246, lot 7; Cell Signaling), mouse monoclonal anti-myc (1:1000, cat. 2276, lot 24; Cell Signaling), rabbit monoclonal anti-SUZ12 (1:1000, cat. 3737, lot 6; Cell Signaling), and anti-EED (1:1000, cat. CS204393; Millipore, St. Louis, MO), rabbit monoclonal anti-H3K27me3 (1:1000, cat. CS200603, lot 2819348; Millipore), mouse monoclonal anti-H3 (1:1000, cat. 14269, lot 1; Cell Signaling), mouse monoclonal anti-STAT3 (1:1000, cat. 9139, lot 10; Cell Signaling), and rabbit monoclonal anti-pSTAT3 (1:100, cat. 9131, lot 30; Cell Signaling).

Plasmids

WT *FOXP3* coding DNA exons (1293 base pairs) were amplified from PBMC-derived human Tregs using primers for BamH1 and Xho1 restriction sites. Digested (Nucleospin Gel and polymerase chain reaction clean-up, Takara, Palo Alto, CA) *FOXP3* DNA then was cloned into pCDNA3.1–His–tagged vector plasmid to generate a fusion of His-tagged FOXP3 (pCDNA3.1–His–FOXP3). Fusion plasmid myc–DDK–tagged human EZH2 was obtained from Origene (cat. RC202054, Rockville, MD), whereas myc–His–tagged human EZH2 was a kind gift from Mien-Chie Hung. The human *IL2* luciferase reporter was purchased from Affymetrix (cat. LR1014).

Flow Cytometry

For cell-surface staining, cells were directly stained with the indicated antibodies in stain buffer (BioLegend). For intracellular staining, cells were treated as indicated with or without brefeldin A (cat. 420601, lot B211242; BioLegend), fixed and permeabilized with buffer (cat. 51-2090KZ, lot 7180887; BD Biosciences) and then stained with relevant primary antibodies and fluorochrome-conjugated secondary antibodies, alternatively, cells were stained with fluorochrome-conjugated primary antibodies. The antibodies used were mouse monoclonal anti-EZH2 (1:100, cat. 3174, lot 4; Cell Signaling), goat anti-mouse IgG (H + L) (1:1000, A21235, lot 1704598; Life Technologies), anti-rat IgG–Alexa Flour 647 (1:1000, cat. 400526, lot B22506; Invitrogen), anti-human FOXP3–Alexa Flour 488 (cat. 320212, lot B231491; BioLegend), mouse monoclonal anti-His–Alexa Flour 488 (cat. A01800, lot 15L000966; GenScript, Piscataway, NJ), anti-human IL2–Alexa Flour 647 (cat. 500315, lot B264459; Biolegend). Cells were washed with staining buffer (cat. 420201, lot B247190; BioLegend) or perm/wash buffer (cat. 51-2091KZ, lot 7311596; BD Biosciences), respectively, to remove unbound antibodies. Cells subsequently were subjected to flow cytometry for fluorescence-activated cell sorting and electronically gated on live cells for analysis.

ChIP Assays

ChIP assays were performed in Jurkat cells (4×10^6) by cross-linking with 1% formaldehyde for 10 minutes at room temperature and then washed with ice-cold PBS supplemented with protease inhibitors. Cells were resuspended in sodium dodecyl sulfate lysis buffer (50 nmol/L Tris-HCl, pH 8.1, 10 mmol/L EDTA, 1% sodium dodecyl sulfate, and protease inhibitors). Lysates were sonicated (40–45 W for 10-second bursts, 8 times on ice) to yield 100–500 bp of chromatin fragments and diluted 10-fold with ChIP dilution buffer (20 mmol/L Tris-HCl, pH 8.1, 1 mmol/L EDTA, 150 mmol/L NaCl, 0.3% Triton X-100, and protease inhibitors). Lysates were precleared with protein A agarose/salmon sperm DNA (cat. 16-157, lot 2798592; Millipore) for 2 hours and then incubated with rabbit monoclonal anti-H3K27me3 (1:1000, cat. 17-622; Millipore) or relevant IgG control overnight, followed by incubation with protein A agarose/salmon sperm DNA for 3 hours at 4°C. Protein A agarose–bound complexes were washed simultaneously with low salt, high salt, and LiCl immune complex wash buffers as well as Tris-EDTA buffer. Antibody/protein/DNA complexes were eluted. Quantitative polymerase chain

reaction was performed for the *IFNγ* promoter (forward primer: 5'-CTGATGAAGGACTTCCTCACC-3'; reverse primer: 5'-CGATGAGACAGACCCATTATGCC-3').

Site-Directed Mutagenesis

DNA base substitutions and deletions were performed using the Q5 site-directed mutagenesis kit (New England Biolabs, Ipswich, MA) according to the manufacturer's instructions. Forward and reverse primer sequences required for specific site mutagenesis were generated using the NEBase Changer tool (Ipswich, MA). Primers used were as follows: FOXP3-C232G (TGT mutation to GGT: cysteine 232 to glycine): forward-CAGGGCACAAGGTC TCCTCCA, reverse-CCCTTCTCATCCAGAAGATGG; FOXP3-C232Δ (TGT deletion: cysteine 232 deletion): forward-CTCCTCCAGAGAGAGATGG, reverse-TTGTGCCCTGCCCTTCTC; FOXP3-L242P (CTG mutation to CCT: leucine 242 to proline): forward-GGTACAGTCTCCTGAGCAGCAGC, reverse-ATCTCTC TCTGGAGGAGAC; and FOXP3-K250Δ (AAG 250 deletion: lysine 250 deletion): forward-GAGAAGCTGAGTGCCATGC, reverse-CTCCAGCACCAGCTGCTG.

Luciferase Reporter Assays

Jurkat T cells were transfected with the indicated constructs (control renilla luciferase and *IL2* firefly luciferase) for 48–72 hours. Cells were treated as indicated, anti-human CD3 (OKT3, 10 μg/mL) and anti-human CD28 (2 μg/mL) or cell activation cocktail containing 0.081 μmol/L PMA and 1.34 μmol/L ionomycin for 12 hours or overnight. Cells also were treated with the EZH2 inhibitor GSK126 (cat. S7061; Selleckchem) as indicated. Cells were harvested and luciferase activity was detected and measured by using the Dual-Luciferase Assay Reporter System kit (E1960, lot 000021191; Promega, Madison, WI) and a Synergy H1-Multi Mode plate reader (BioTek, Winooski, VT) according to the manufacturer's instructions.

References

1. Cho JH, Feldman M. Heterogeneity of autoimmune diseases: pathophysiologic insights from genetics and implications for new therapies. Nat Med 2015;21:730–738.
2. Cho JH. The genetics and immunopathogenesis of inflammatory bowel disease. Nat Rev Immunol 2008; 8:458–466.
3. McGovern DP, Kugathasan S, Cho JH. Genetics of inflammatory bowel diseases. Gastroenterology 2015; 149:1163–1176.e2.
4. Hunter CA, Jones SA. IL-6 as a keystone cytokine in health and disease. Nat Immunol 2015;16:448–457.
5. Isaacs KL, Sartor RB, Haskill S. Cytokine messenger RNA profiles in inflammatory bowel disease mucosa detected by polymerase chain reaction amplification. Gastroenterology 1992;103:1587–1595.
6. Reinecker HC, Steffen M, Witthoeft T, Pflueger I, Schreiber S, MacDermott RP, Raedler A. Enhanced secretion of tumour necrosis factor-alpha, IL-6, and IL-1 beta by isolated lamina propria mononuclear cells from patients with ulcerative colitis and Crohn's disease. Clin Exp Immunol 1993;94:174–181.
7. Holub MC, Mako E, Devay T, Dank M, Szalai C, Fenyvesi A, Falus A. Increased interleukin-6 levels, interleukin-6 receptor and gp130 expression in peripheral lymphocytes of patients with inflammatory bowel disease. Scand J Gastroenterol Suppl 1998;228:47–50.
8. Hosokawa T, Kusugami K, Ina K, Ando T, Shinoda M, Imada A, Ohsuga M, Sakai T, Matsuura T, Ito K, Kaneshiro K. Interleukin-6 and soluble interleukin-6 receptor in the colonic mucosa of inflammatory bowel disease. J Gastroenterol Hepatol 1999;14:987–996.
9. Gross V, Andus T, Caesar I, Roth M, Scholmerich J. Evidence for continuous stimulation of interleukin-6 production in Crohn's disease. Gastroenterology 1992; 102:514–519.
10. Roda G, Jharap B, Neeraj N, Colombel JF. Loss of response to anti-TNFs: definition, epidemiology, and management. Clin Transl Gastroenterol 2016;7:e135.
11. Coskun M, Vermeire S, Nielsen OH. Novel targeted therapies for inflammatory bowel disease. Trends Pharmacol Sci 2017;38:127–142.
12. Ohkura N, Kitagawa Y, Sakaguchi S. Development and maintenance of regulatory T cells. Immunity 2013; 38:414–423.
13. Sakaguchi S. Naturally arising Foxp3-expressing CD25+CD4+ regulatory T cells in immunological tolerance to self and non-self. Nat Immunol 2005;6:345–352.
14. Josefowicz SZ, Lu LF, Rudensky AY. Regulatory T cells: mechanisms of differentiation and function. Annu Rev Immunol 2012;30:531–564.
15. Kim JM, Rasmussen JP, Rudensky AY. Regulatory T cells prevent catastrophic autoimmunity throughout the lifespan of mice. Nat Immunol 2007;8:191–197.
16. Bennett CL, Christie J, Ramsdell F, Brunkow ME, Ferguson PJ, Whitesell L, Kelly TE, Saulsbury FT, Chance PF, Ochs HD. The immune dysregulation, polyendocrinopathy, enteropathy, X-linked syndrome (IPEX) is caused by mutations of FOXP3. Nat Genet 2001; 27:20–21.
17. Bennett CL, Brunkow ME, Ramsdell F, O'Briant KC, Zhu Q, Fuleihan RL, Shigeoka AO, Ochs HD, Chance PF. A rare polyadenylation signal mutation of the FOXP3 gene (AAUAAA–>AAUGAA) leads to the IPEX syndrome. Immunogenetics 2001;53:435–439.
18. Chatila T. The regulatory T cell transcriptosome: E pluribus unum. Immunity 2007;27:693–695.
19. Rudra D, deRoos P, Chaudhry A, Niec RE, Arvey A, Samstein RM, Leslie C, Shaffer SA, Goodlett DR, Rudensky AY. Transcription factor Foxp3 and its protein partners form a complex regulatory network. Nat Immunol 2012;13:1010–1019.
20. Pan F, Yu H, Dang EV, Barbi J, Pan X, Grosso JF, Jinasena D, Sharma SM, McCadden EM, Getnet D, Drake CG, Liu JO, Ostrowski MC, Pardoll DM. Eos mediates Foxp3-dependent gene silencing in CD4+ regulatory T cells. Science 2009;325:1142–1146.
21. Gandhi R, Kumar D, Burns EJ, Nadeau M, Dake B, Laroni A, Kozoriz D, Weiner HL, Quintana FJ. Activation of the aryl hydrocarbon receptor induces human type 1

regulatory T cell-like and Foxp3(+) regulatory T cells. Nat Immunol 2010;11:846–853.
22. Ichiyama K, Yoshida H, Wakabayashi Y, Chinen T, Saeki K, Nakaya M, Takaesu G, Hori S, Yoshimura A, Kobayashi T. Foxp3 inhibits RORgammat-mediated IL-17A mRNA transcription through direct interaction with RORgammat. J Biol Chem 2008;283:17003–17008.
23. Bettelli E, Dastrange M, Oukka M. Foxp3 interacts with nuclear factor of activated T cells and NF-kappa B to repress cytokine gene expression and effector functions of T helper cells. Proc Natl Acad Sci U S A 2005; 102:5138–5143.
24. Li B, Samanta A, Song X, Iacono KT, Bembas K, Tao R, Basu S, Riley JL, Hancock WW, Shen Y, Saouaf SJ, Greene MI. FOXP3 interactions with histone acetyltransferase and class II histone deacetylases are required for repression. Proc Natl Acad Sci U S A 2007;104:4571–4576.
25. Zhang F, Meng G, Strober W. Interactions among the transcription factors Runx1, RORgammat and Foxp3 regulate the differentiation of interleukin 17-producing T cells. Nat Immunol 2008;9:1297–1306.
26. Kouzarides T. Chromatin modifications and their function. Cell 2007;128:693–705.
27. Portela A, Esteller M. Epigenetic modifications and human disease. Nat Biotechnol 2010;28:1057–1068.
28. DuPage M, Chopra G, Quiros J, Rosenthal WL, Morar MM, Holohan D, Zhang R, Turka L, Marson A, Bluestone JA. The chromatin-modifying enzyme Ezh2 is critical for the maintenance of regulatory T cell identity after activation. Immunity 2015;42:227–238.
29. Sarmento OF, Svingen PA, Xiong Y, Sun Z, Bamidele AO, Mathison AJ, Smyrk TC, Nair AA, Gonzalez MM, Sagstetter MR, Baheti S, McGovern DP, Friton JJ, Papadakis KA, Gautam G, Xavier RJ, Urrutia RA, Faubion WA. The role of the histone methyltransferase enhancer of zeste homolog 2 (EZH2) in the pathobiological mechanisms underlying inflammatory bowel disease (IBD). J Biol Chem 2017;292:706–722.
30. Barski A, Cuddapah S, Cui K, Roh TY, Schones DE, Wang Z, Wei G, Chepelev I, Zhao K. High-resolution profiling of histone methylations in the human genome. Cell 2007;129:823–837.
31. Yang XP, Jiang K, Hirahara K, Vahedi G, Afzali B, Sciume G, Bonelli M, Sun HW, Jankovic D, Kanno Y, Sartorelli V, O'Shea JJ, Laurence A. EZH2 is crucial for both differentiation of regulatory T cells and T effector cell expansion. Sci Rep 2015;5:10643.
32. Glocker EO, Kotlarz D, Boztug K, Gertz EM, Schaffer AA, Noyan F, Perro M, Diestelhorst J, Allroth A, Murugan D, Hatscher N, Pfeifer D, Sykora KW, Sauer M, Kreipe H, Lacher M, Nustede R, Woellner C, Baumann U, Salzer U, Koletzko S, Shah N, Segal AW, Sauerbrey A, Buderus S, Snapper SB, Grimbacher B, Klein C. Inflammatory bowel disease and mutations affecting the interleukin-10 receptor. N Engl J Med 2009;361:2033–2045.
33. Glocker EO, Frede N, Perro M, Sebire N, Elawad M, Shah N, Grimbacher B. Infant colitis–it's in the genes. Lancet 2010;376:1272.
34. Zeissig S, Petersen BS, Tomczak M, Melum E, Huc-Claustre E, Dougan SK, Laerdahl JK, Stade B, Forster M, Schreiber S, Weir D, Leichtner AM, Franke A, Blumberg RS. Early-onset Crohn's disease and autoimmunity associated with a variant in CTLA-4. Gut 2015; 64:1889–1897.
35. Okou DT, Mondal K, Faubion WA, Kobrynski LJ, Denson LA, Mulle JG, Ramachandran D, Xiong Y, Svingen P, Patel V, Bose P, Waters JP, Prahalad S, Cutler DJ, Zwick ME, Kugathasan S. Exome sequencing identifies a novel FOXP3 mutation in a 2-generation family with inflammatory bowel disease. J Pediatr Gastroenterol Nutr 2014;58:561–568.
36. Arvey A, van der Veeken J, Samstein RM, Feng Y, Stamatoyannopoulos JA, Rudensky AY. Inflammation-induced repression of chromatin bound by the transcription factor Foxp3 in regulatory T cells. Nat Immunol 2014;15:580–587.
37. Lopes JE, Torgerson TR, Schubert LA, Anover SD, Ocheltree EL, Ochs HD, Ziegler SF. Analysis of FOXP3 reveals multiple domains required for its function as a transcriptional repressor. J Immunol 2006; 177:3133–3142.
38. Song X, Li B, Xiao Y, Chen C, Wang Q, Liu Y, Berezov A, Xu C, Gao Y, Li Z, Wu SL, Cai Z, Zhang H, Karger BL, Hancock WW, Wells AD, Zhou Z, Greene MI. Structural and biological features of FOXP3 dimerization relevant to regulatory T cell function. Cell Rep 2012;1:665–675.
39. Bandukwala HS, Wu Y, Feuerer M, Chen Y, Barboza B, Ghosh S, Stroud JC, Benoist C, Mathis D, Rao A, Chen L. Structure of a domain-swapped FOXP3 dimer on DNA and its function in regulatory T cells. Immunity 2011; 34:479–491.
40. Bruniquel D, Schwartz RH. Selective, stable demethylation of the interleukin-2 gene enhances transcription by an active process. Nat Immunol 2003; 4:235–240.
41. Li B, Samanta A, Song X, Iacono KT, Brennan P, Chatila TA, Roncador G, Banham AH, Riley JL, Wang Q, Shen Y, Saouaf SJ, Greene MI. FOXP3 is a homo-oligomer and a component of a supramolecular regulatory complex disabled in the human XLAAD/IPEX autoimmune disease. Int Immunol 2007;19:825–835.
42. Chae WJ, Henegariu O, Lee SK, Bothwell AL. The mutant leucine-zipper domain impairs both dimerization and suppressive function of Foxp3 in T cells. Proc Natl Acad Sci U S A 2006;103:9631–9636.
43. Wang B, Lin D, Li C, Tucker P. Multiple domains define the expression and regulatory properties of Foxp1 forkhead transcriptional repressors. J Biol Chem 2003; 278:24259–24268.
44. Mackey-Cushman SL, Gao J, Holmes DA, Nunoya JI, Wang R, Unutmaz D, Su L. FoxP3 interacts with linker histone H1.5 to modulate gene expression and program Treg cell activity. Genes Immun 2011;12:559–567.
45. van Loosdregt J, Coffer PJ. Post-translational modification networks regulating FOXP3 function. Trends Immunol 2014;35:368–378.
46. Ding X, Wang A, Ma X, Demarque M, Jin W, Xin H, Dejean A, Dong C. Protein SUMOylation is required for regulatory T cell expansion and function. Cell Rep 2016; 16:1055–1066.

47. Hedrick SM, Hess Michelini R, Doedens AL, Goldrath AW, Stone EL. FOXO transcription factors throughout T cell biology. Nat Rev Immunol 2012;12:649–661.
48. Bour-Jordan H, Bluestone JA. Regulating the regulators: costimulatory signals control the homeostasis and function of regulatory T cells. Immunol Rev 2009; 229:41–66.
49. La Cava A. Tregs are regulated by cytokines: implications for autoimmunity. Autoimmun Rev 2008;8:83–87.
50. Korn T, Mitsdoerffer M, Croxford AL, Awasthi A, Dardalhon VA, Galileos G, Vollmar P, Stritesky GL, Kaplan MH, Waisman A, Kuchroo VK, Oukka M. IL-6 controls Th17 immunity in vivo by inhibiting the conversion of conventional T cells into Foxp3+ regulatory T cells. Proc Natl Acad Sci U S A 2008;105:18460–18465.
51. Goodman WA, Levine AD, Massari JV, Sugiyama H, McCormick TS, Cooper KD. IL-6 signaling in psoriasis prevents immune suppression by regulatory T cells. J Immunol 2009;183:3170–3176.
52. Chen X, Das R, Komorowski R, Beres A, Hessner MJ, Mihara M, Drobyski WR. Blockade of interleukin-6 signaling augments regulatory T-cell reconstitution and attenuates the severity of graft-versus-host disease. Blood 2009;114:891–900.
53. Winthrop KL. The emerging safety profile of JAK inhibitors in rheumatic disease. Nat Rev Rheumatol 2017; 13:320.
54. Schoepfer AM, Beglinger C, Straumann A, Trummler M, Vavricka SR, Bruegger LE, Seibold F. Fecal calprotectin correlates more closely with the Simple Endoscopic Score for Crohn's disease (SES-CD) than CRP, blood leukocytes, and the CDAI. Am J Gastroenterol 2010;105:162–169.
55. Hayatsu N, Miyao T, Tachibana M, Murakami R, Kimura A, Kato T, Kawakami E, Endo TA, Setoguchi R, Watarai H, Nishikawa T, Yasuda T, Yoshida H, Hori S. Analyses of a mutant Foxp3 allele reveal BATF as a critical transcription factor in the differentiation and accumulation of tissue regulatory T cells. Immunity 2017; 47:268–283.e9.
56. Mottet C, Uhlig HH, Powrie F. Cutting edge: cure of colitis by CD4+CD25+ regulatory T cells. J Immunol 2003;170:3939–3943.
57. Read S, Powrie F. Induction of inflammatory bowel disease in immunodeficient mice by depletion of regulatory T cells. Curr Protoc Immunol 2001;15:Unit 15.13.
58. Ishikawa D, Okazawa A, Corridoni D, Jia LG, Wang XM, Guanzon M, Xin W, Arseneau KO, Pizarro TT, Cominelli F. Tregs are dysfunctional in vivo in a spontaneous murine model of Crohn's disease. Mucosal Immunol 2013; 6:267–275.
59. Saruta M, Yu QT, Fleshner PR, Mantel PY, Schmidt-Weber CB, Banham AH, Papadakis KA. Characterization of FOXP3+CD4+ regulatory T cells in Crohn's disease. Clin Immunol 2007;125:281–290.
60. Kelsen J, Agnholt J, Hoffmann HJ, Romer JL, Hvas CL, Dahlerup JF. FoxP3(+)CD4(+)CD25(+) T cells with regulatory properties can be cultured from colonic mucosa of patients with Crohn's disease. Clin Exp Immunol 2005; 141:549–557.
61. Makita S, Kanai T, Oshima S, Uraushihara K, Totsuka T, Sawada T, Nakamura T, Koganei K, Fukushima T, Watanabe M. CD4+CD25bright T cells in human intestinal lamina propria as regulatory cells. J Immunol 2004; 173:3119–3130.
62. Heink S, Yogev N, Garbers C, Herwerth M, Aly L, Gasperi C, Husterer V, Croxford AL, Moller-Hackbarth K, Bartsch HS, Sotlar K, Krebs S, Regen T, Blum H, Hemmer B, Misgeld T, Wunderlich TF, Hidalgo J, Oukka M, Rose-John S, Schmidt-Supprian M, Waisman A, Korn T. Trans-presentation of IL-6 by dendritic cells is required for the priming of pathogenic T_H17 cells. Nat Immunol 2017;18:474.
63. Kitani A, Xu L. Regulatory T cells and the induction of IL-17. Mucosal Immunol 2008;1(Suppl 1):S43–S46.
64. Nie H, Zheng Y, Li R, Guo TB, He D, Fang L, Liu X, Xiao L, Chen X, Wan B, Chin YE, Zhang JZ. Phosphorylation of FOXP3 controls regulatory T cell function and is inhibited by TNF-alpha in rheumatoid arthritis. Nat Med 2013; 19:322–328.
65. Levine AG, Mendoza A, Hemmers S, Moltedo B, Niec RE, Schizas M, Hoyos BE, Putintseva EV, Chaudhry A, Dikiy S, Fujisawa S, Chudakov DM, Treuting PM, Rudensky AY. Corrigendum: stability and function of regulatory T cells expressing the transcription factor T-bet. Nature 2017;550:142.
66. Ito H, Takazoe M, Fukuda Y, Hibi T, Kusugami K, Andoh A, Matsumoto T, Yamamura T, Azuma J, Nishimoto N, Yoshizaki K, Shimoyama T, Kishimoto T. A pilot randomized trial of a human anti-interleukin-6 receptor monoclonal antibody in active Crohn's disease. Gastroenterology 2004;126:989–996; discussion 47.

Received January 9, 2018. Accepted August 30, 2018.

Correspondence
Address correspondence to: William A. Faubion Jr, MD, Division of Gastroenterology and Hepatology, Mayo Clinic, 200 First Street SW, Guggenheim Building, Room 10-24, Rochester, Minnesota 55905. e-mail: Faubion.William@mayo.edu; fax: (507) 255-6318.

Acknowledgments
The authors thank the Mayo Clinic Flow Cytometry Core Facility for expert and technical assistance and Dr Laura Raffals and Jessica Friton for assistance in obtaining human biopsy specimens.

Author contributions
Adebowale O. Bamidele was responsible for the study concept and design, data acquisition, data analysis and interpretation, and manuscript preparation; Phyllis A. Svingen was responsible for data acquisition and manuscript preparation and revision; Michelle Gonzalez, Mary R. Sagstetter, Olga F. Sarmento, and Manuel B. Braga Neto acquired and interpreted data; Raul A. Urrutia, Subra Kugathasan, and Gwen Lomberk interpreted data and prepared the manuscript; and William A. Faubion Jr was responsible for study supervision, the study concept and design, data analysis and interpretation, manuscript preparation, and acquired funding.

Conflicts of interest
The authors disclose no conflicts.

Funding
This work was supported by National Institute of Diabetes and Digestive and Kidney Diseases training grant T32DK007198 and the Pilot and Feasibility Award by the Center for Cell Signaling in Gastroenterology (P30DK084567) (A.O.B.), the National Institutes of Health National Institute of Diabetes and Digestive and Kidney Diseases RO1 grant DK52913 (R.A.U.), and the National Institute of Allergy and Infectious Diseases RO1 grant AI089714 and the Leona Helmsley Charitable Trust (W.A.F.).